Image Recovery: Theory and Applications, H. Stark, ed.
pp. 79-125 (Academic, Orlando, 1987)

CHAPTER 3

Bayesian and Related Methods in Image Reconstruction from Incomplete Data

Kenneth M. Hanson

Los Alamos National Laboratory
Los Alamos, New Mexico 87545

3.1 INTRODUCTION

The problem of obtaining an artifact-free computed tomographic (CT) reconstruction from projection data that are limited in number and possibly angular coverage is a difficult one to solve in general. Similarly, restorations of blurred images are almost always marred by artifacts that appear to be related to the blurring function. These difficulties arise from a fundamental limitation inherent in incomplete data sets. This limitation may be viewed as resulting from an essential lack of information in the measurements about the unknown source function, which is codified in the concept of the null space of functions associated with the measurement geometry. The Bayesian approach allows one to incorporate *a priori* information about the source function based on the properties of the ensemble of source functions realizable in the specified imaging situation. If the prior knowledge is restrictive enough, reasonable estimates of the null-space components of the source function can be obtained, thereby reducing the artifacts in the reconstruction. The use of prior knowledge about the shape or structure of the source function will be emphasized here. The results of the maximum *a posteriori* (MAP) method will be compared with the fit and iterative reconstruction (FAIR) technique, in which the previously known shape of the object may be explicitly incorporated by means of a model of the object.

Copyright 1987 by Academic Press, Inc
All rights of reproduction in any form reserved

Finally, a more comprehensive and flexible Bayesian approach is suggested in which the ensemble mean and covariance specifications are estimated with the help of the measurements.

The present work deals with discretely sampled, linear imaging systems. Thus, the concept of null space and the Bayesian methods proposed for overcoming its limitations are relevant to a wide variety of digital image restoration problems. The term reconstruction will be used here to refer to image recovery in a broad sense, encompassing, for example, tomographic reconstruction, restoration of blurred images, and decoding of encoded images. Owing to the background of the author and the basis of this chapter on an earlier article related to tomography [1], the discussion is heavily weighted toward tomographic reconstruction.

3.2 MEASUREMENT SPACE—NULL SPACE

The CT reconstruction problem may be stated as follows: given a finite set of projections of a function of two dimensions $f(x, y)$ with compact support, obtain the best estimate of that function. Each projection may generally be written as a weighted two-dimensional (2-D) integral of $f(x, y)$

$$g_i = \iint_{-\infty}^{\infty} h_i(x, y) f(x, y) \, dx \, dy, \qquad (3.2\text{-}1)$$

where the h_i are the weighting functions and $i = 1, 2, \ldots, N$ for N individual measurements. We will refer to the h_i as response functions. In the CT problem, the h_i typically have large values within a narrow strip and small or zero values outside the strip. If the h_i are unity within a strip of finite width and are zero outside, Eq. (3.2-1) becomes a strip integral. For zero strip width, it becomes a line integral. These are recognized as idealizations of the usual physical situation. The generality of Eq (3.2-1) allows it to closely represent actual physical measurements because it can take into account response functions that vary with position. For example, a slowly increasing strip width is implied by the divergence of the sampling beam inherent in proton computed tomography [2, 3], in diffraction tomography with ultrasound [4], which is discussed by Kaveh and Somekh in Chapter 10, or in well-to-well seismic tomography [5].

Equation (3.2-1) is clearly applicable to any discretely sampled, linear imaging system. What will be developed regarding the CT problem will therefore be applicable to the *image recovery problem* in general. For example, Eq. (3.2-1) applies to the standard reconstruction problem in image processing of the restoration of an image from its blurred rendition. In this case, each g_i is a sample of the blurred image and the response function $h_i(x, y)$ is the blur function, which defines how much the intensity of the original image f at each point (x, y) contributes to g_i. The CT problem may be thought of as a special case of the general image recovery problem in which the blur function is a thin strip that transverses the region of support.

It is often convenient to use vector notation to express relationships in linear imaging systems [6]. Assume the unknown function $f(x, y)$ and the response functions $h_i(x, y)$ belong to a Hilbert vector space (Chapter 1). Then Eq. (3.2-1) is identified as an inner product between the vectors $\mathbf{h}_i$ and $\mathbf{f}$. This may be expressed in vector notation as

$$g_i = (\mathbf{h}_i, \mathbf{f}) = \mathbf{h}_i^T\mathbf{f}, \tag{3.2-2}$$

where $(\mathbf{a}, \mathbf{b})$ denotes the inner product between vectors $\mathbf{a}$ and $\mathbf{b}$ and the superscript T denotes the transpose operation, which converts a column vector into a row vector. All N equations implied by Eq. (3.2-1) may be summarized as

$$\mathbf{g} = \mathbf{H}\mathbf{f}. \tag{3.2-3}$$

In the present context, $\mathbf{H}$ is interpreted as a linear operator corresponding to the measurement process, which maps the function $f(x, y)$ defined on the 2-D continuous domain of (x, y) onto the discrete set of measurements enumerated by the index i.

Returning to Eq. (3.2-2), each measurement g_i may be thought of as a projection of the unknown vector $\mathbf{f}$ onto the response vector $\mathbf{h}_i$. Only those components of $\mathbf{f}$ that lie in the subspace spanned by the set of all $\mathbf{h}_i$ contribute to the measurements. This subspace will be called the *measurement space.* The components of $\mathbf{f}$ in the remaining orthogonal subspace, the *null space,* do not contribute to the measurements. Any vector lying wholly in the null space yields zero for all measurements. As a consequence, the null-space contribution to $\mathbf{f}$ cannot be determined from the measurements alone. The fact that $f(x, y)$ is a function of the continuous variables x and y implies that $\mathbf{f}$ must belong to a vector space of infinite dimensions. A finite number of measurements can only provide information about a finite-dimensional subspace of the infinite-dimensional space of $\mathbf{f}$. In such circumstances, the null space must have infinite dimension! Therefore, given a finite number of measurements, it is never possible to completely determine an arbitrary $f(x, y)$. Hence, the seemingly frivolous statement "a finite set of radiographs tells nothing at all" [7] about a 3-D object. Virtually every digital image recovery problem possesses a null space.

The ambiguities associated with the existence of a null space arise because of the many-to-one (infinite-to-one) transformation from the original object to the finite number of measurements, which is inherently noninvertable. When a null space exists, the data are said to be incomplete. In other terminology, the inability to determine a correct solution to the measurement equations, Eq. (3.2-1), is called an ill-posed problem. Further reading on the null-space/measurement-space concept may be found in papers by Twomey [8–10], Tanabe [11], Jackson [12], Katz [13], Llacer [14], and Sanz and Huang [15].

Figure 3.2-1 illustrates that the null-space component of an image is a tangible entity, which is easily calculable. It is assumed that measurements are available along 11 projection directions, which span only 90° in view angle. Figure 3.2-1c is obtained by starting the algebraic reconstruction technique (ART) algorithm [16] with the source distribution of Fig. 3.2-1a and using zero for all the assumed projection measurements. On convergence ART produces an image whose projections match the input values, that is, zero, along each of the 11 assumed projection directions. As explained in the next section, ART affects only the measurement-space component of the image, leaving just the null-space component in this case. Figure 3.2-1c is just one of many possible null-space images that will not contribute anything to the available measurements in the assumed projection directions. The difference between Figs. 3.2-1a and 3.2-1c is the measurement-space component of the source, Fig. 3.2-1b, which is unambiguously determined by noiseless projection measurements. As explained below, this should be the result obtained by using standard, deterministic reconstruction algorithms whose solutions satisfy the measurement Eqs. (3.2-1).

Other authors have alluded to the problem of the null space in CT [17, 18] but have not explicitly considered its visual effect on reconstructions from limited projection data. The existence of the ambiguities associated with the null space is known well by applied mathematicians. For example, the range of the transpose of the projection-measurement matrix A, referred to by Lakshminarayan and Lent [18] in stating the restrictions to their Theorem 1, which concerns the convergence of Richardson's algorithm, is the measurement space in their square-pixel representation.

Specific discussion of the null space associated with the CT problem has appeared in many articles. Smith *et al.* [7] explored the null space of a finite number of projections to determine the convergence rate of the ART algorithm. This work was extended by Hamaker and Solmon [19], who went so far as to calculate the "angles" between the null spaces corresponding to such projections. Katz [13] made extensive use of the null-space concept to determine the conditions for uniqueness of a reconstruction, since the original function $f(x, y)$ can be unambiguously determined if and only if the null space associated with the measurements is empty (his Proposition VI.1). Louis [20] developed an explicit expression for functions

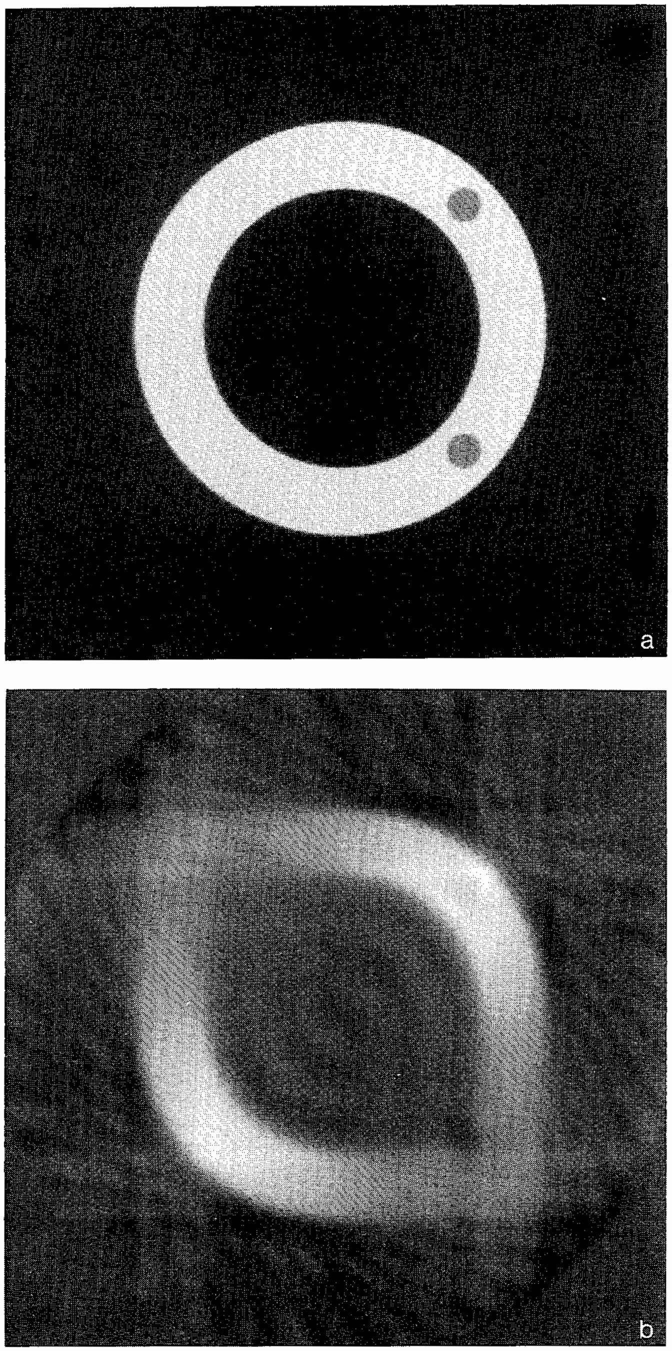
a
b

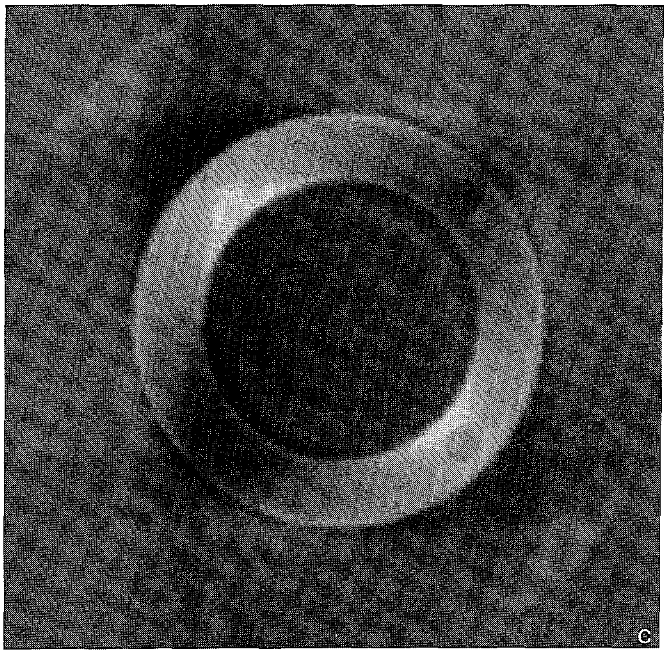

(*continued*)

belonging to the null space corresponding to a finite number of evenly spaced projections and showed that ghosts from the null space could appear as lesions. Louis [21] also considered the null space associated with projection imaging in higher dimensions and developed suitable series expansions. Medoff *et al.* [22, 23] recognized the consequences of the null space associated with limited data and introduced a method to reduce null-space ghosts through the application of known constraints on the reconstructed image. Further references on the limited-angle CT problem may be found in [24]. Andrews and Hunt [6] offer numerous cogent discussions of the difficulties introduced by the null space in image restoration without mentioning it by name. The importance of the null-space problem in other image inversion problems will be discussed in the next section.

Fig. 3.2-1. Decomposition of an object consisting of an annulus with two half-density holes (a) into its measurement-space (b) and null-space (c) contributions corresponding to the assumption that there are 11 measured projections available covering 90°. The projections of (c) along each of the 11 measurement directions are zero! This illustrates that for any given measurement scheme, every function is a sum of a component that is measured and a component that is not.

Fourier analysis is often used to visualize the CT problem. Its usefulness stems from the *projection-slice theorem*, which states that the 1-D Fourier transform of a projection taken with parallel strip or line integrals is the same as the 2-D Fourier transform of $f(x, y)$ evaluated along a line through the origin of the 2-D spatial-frequency domain. See Chapters 9, 10, and 11. Then the knowledge of a set of parallel projections that span a limited range of angles is tantamount to knowing the Fourier amplitudes of the object inside the corresponding sector of the 2-D frequency domain. The limited-angle reconstruction problem amounts to determining the Fourier amplitudes in the "missing" sector.

3.3 DETERMINISTIC SOLUTIONS

Deterministic solutions to the measurement Eq. (3.2-1) are defined as solutions that follow directly from the measurements and not from any other information. They typically do not take into account the effect of random noise, which is always present in actual measurements. As argued in the previous section, deterministic solutions should be restricted to the measurement space. This restriction will now be explored for many of the standard methods used to solve the image recovery problem.

It is natural to expand the estimate of $f(x, y)$ in terms of the response functions [25]

$$\hat{f}(x, y) = \sum_{i=1}^{N} a_i h_i(x, y). \tag{3.3-1}$$

Since the measurement subspace of $f(x, y)$ is spanned by the response functions, this expansion provides a complete basis for the measurement space. Because the $h_i(x, y)$ are orthogonal to the null space, the null-space components of $\hat{f}(x, y)$ are zero. This leads to artifacts in $\hat{f}(x, y)$ because it does not possess those components of the original function $f(x, y)$ that lie in the null space [24]. In vector notation Eq. (3.3-1) may be expressed as

$$\hat{\mathbf{f}} = \mathbf{H}^T \mathbf{a}, \tag{3.3-2}$$

where $\mathbf{a}$ is the vector of length N composed of the coefficients a_i and $\mathbf{H}^T$ is the transpose of $\mathbf{H}$.

The response function expansion, Eq. (3.3-1), is formally identical to the familiar *backprojection* process [26] where the value a_i is added to the image along the strip function $h_i(x, y)$. The transverse profile of the response function corresponds to the interpolation function used by the backprojection algorithm. In vector notation the backprojection operation is denoted by $\mathbf{H}^T$. Since the response functions are orthogonal to the null space, any backprojection process that includes just the available measurements can only affect the measurement-space components of the reconstruction.

One way often used to overcome the nonuniqueness difficulty associated with the existence of a null space is to seek that solution of Eq. (3.2-1) with minimum norm. This amounts to minimizing

$$\|\hat{f}(x, y)\|^2 = \iint\limits_{-\infty}^{\infty} \hat{f}^2(x, y)\, dx\, dy \qquad (3.3\text{-}3)$$

subject to satisfying all N constraints implied by Eq. (3.2-1). When this minimization problem is approached by the usual method of Lagrange multipliers, it is found that the solution must have the *form* given by Eq. (3.3-1). This is understandable since a necessary condition for its minimum-norm solution is that its null-space components are zero. In the desire to force a unique solution to the inversion problem, the fundamental ambiguities associated with the null space have been glossed over.

In most of the well-known CT reconstruction algorithms, the reconstruction is a linear combination of backprojections. These include filtered backprojection [27], algebraic reconstruction technique (ART) [16, 28], simultaneous iterative reconstruction technique (SIRT) [29], SIRT-like algorithms (least squares [30] and other variants [31]), and the "natural-pixel" matrix formulation by Buonocore *et al.* [25], based explicitly on the expansion given by Eq. (3.3-1). Such algorithms can only alter the measurement-space part of the initial estimate. When the initial estimate lies solely in the measurement space, as is normally the case, so will the final estimate. Then the null-space components of the solution will be zero, leading to artifacts.

Although it is feasible to consider the original function $\mathbf{f}$ to belong to a (Hilbert) vector space of infinite dimensions, it is more typical to limit the dimensionality of the estimate $\hat{\mathbf{f}}$ by writing it as a linear combination of a finite number of basis functions. A common choice for basis functions is that of square pixels placed on an equally spaced grid [6]. In this case, the continuous coordinates x and y in Eq. (3.2-1) are replaced by a single index j designating the jth pixel, the integration becomes a summation, and $\mathbf{H}$ is a matrix. Then the image is represented by the sequence of coefficients that describe each pixel's contribution to the image. This vector of coefficients is often referred to as the image and is denoted by $\hat{\mathbf{f}}$, thereby leaving the vector equations that describe the linear imaging system unchanged. This finite vector belongs to a Euclidean vector space. Other types of local basis functions have considerable merit [32]. In the image-deblurring problem, the sampled data typically consist of a blurred image of the same size as the desired deblurred image. Then $\mathbf{H}$ is a square matrix. In the CT problem, the projection measurements lie in an obviously different domain than the original image. The matrix **H** is very seldom square. The incongruity of the measurement samples and the image that is peculiar to the CT problem make it pedagogically useful for exploring new approaches to image recovery.

The difficulty of inverting the matrix Eq. (3.2-3) for image recovery has been appreciated for some time. The straightforward solution may be written in terms of a matrix inverse

$$\mathbf{f} = \mathbf{H}^{-1}\mathbf{g}. \tag{3.3-4}$$

The inverse exists, however, only if **H** is nonsingular, that is, possesses no null space. An illuminating way to approach the inversion of Eq. (3.2-3) is to consider the singular-value decomposition (SVD) of the measurement matrix **H** (Chapter 1). The number of nonzero singular values gives the rank of **H**, which corresponds to the number of linearly independent measurements of **f**. This has been called the number of degrees of freedom contained in the measurements [6] and is the same as the dimension of the measurement space. The singular vectors of the SVD with zero singular values span the null space. For the purpose of providing an inverse that involves only the measurement space, a *pseudoinverse* can be defined as an expansion of the inverse in terms of singular vectors with nonzero singular values [33]. As an example of the usefulness of this approach, McCaughey and Andrews [34] have calculated the eigenvalue map, which is the sequential ordering of the eigenvalues, of $\mathbf{HH}^T$ for equally spaced projection measurements. Their result for 32 samples per view, Fig. 3.3-1, shows that the number of degrees of freedom asymptotically approaches an upper limit of about 700 as the number of projection angles continually increases. This indicates that the dimension of the measurement space reaches an upper limit and that more projections than roughly 40 do not add much information (in the absence of noise considerations).

It is known that the Fourier analysis of a blurred image with a stationary point spread function (PSF) is closely related to the abovementioned eigenanalysis [6]. In fact, in the circulant approximation of the square, block-Toeplitz matrix **H**, the Fourier transform coefficients of the PSF, called the optical transfer function (OTF), are the eigenvalues of **H**. The zeros in the OTF are identified as being associated with the eigenvectors that span the null space of the PSF. It is this null space that is responsible for artifacts in deterministic reconstructions, which are seen clearly in restorations of blurred text [35]. When several blurred images of the same text are available, each subjected to a different PSF, the reconstruction can be nearly artifact-free [36] because the zeros of the OTSs have little overlap, leaving an almost empty null space.

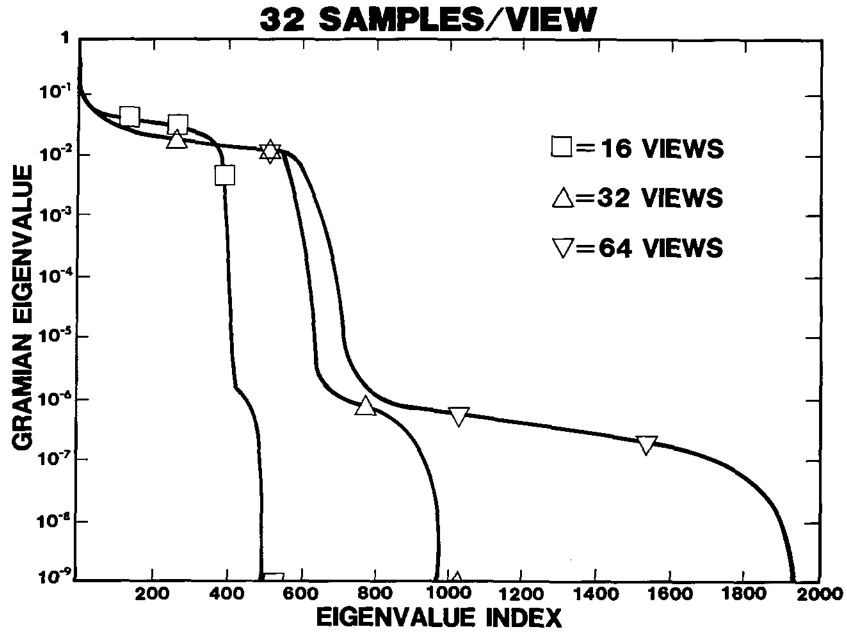

Fig. 3.3-1. Eigenvalue map corresponding to various numbers of equally spaced projections, each consisting of 32 samples. (From McCaughey and Andrews [34]. Copyright 1979 IEEE.)

Many standard deterministic algorithms applied to image recovery have no effect on the null-space component of the solution. For example, when the blur function is symmetric and stationary in the standard problem of the restoration of a blurred image, the response-function expansion, Eq. (3.3-1) or (3.3-2) or the $\mathbf{H}^T$ operation, amounts to a convolution with the blur function itself. Although restoration algorithms are not ordinarily expressed explicitly in terms of such a convolution, all deterministic restoration algorithms can be. In its complete form, the *Wiener filter* [6] is based on the Bayesian approach (next section). However, as it is often applied, the image and noise covariance matrices are assumed to be proportional to the identity matrix, reflecting a lack of prior knowledge. In this case the Wiener filter leaves zeros in the OTF unchanged. Thus the null-space component of $\hat{\mathbf{f}}$ is zero and it must lie in the measurement space. As such, it can be written as an expansion in terms of the response functions, that is, as Eq. (3.2-2). The same can be said of the homomorphic filter. Pseudoinverse methods, when expressed in terms of the singular vectors of $\mathbf{H}$, avoid the use of singular vectors with zero singular values, again leaving the null-space components zero. In the constrained least-squares approach, the norm of some linear operator times $\mathbf{f}$ is minimized subject to the condition that χ^2 (see next section) be equal to a prescribed value. It can be shown that when the operator is diagonal, the reconstruction is proportional to $\mathbf{H}^T$. When the operator is not diagonal, the null space can be impacted, but this nondiagonality implies the use of specific prior knowledge and the algorithm cannot be viewed as deterministic. It is concluded that deterministic restoration algorithms do not affect the null-space component of the unblurred image.

The restriction of deterministic solutions to the measurement space should not be viewed as a negative conclusion. Rather, it is simply a statement of what is possible for a given set of measurements in the absence of further information. It allows one formally to reinterpret the goal for obtaining an improved reconstruction from limited data as that of estimating the null-space contribution through the use of further information available about the function to be reconstructed.

3.4 THE BAYESIAN APPROACH

The essence of the Bayesian approach is the assumption that the image to be reconstructed is a random selection from an identifiable ensemble of similar images. In the context of medical imaging, an example of such an ensemble is the collection of all hearts imaged by the same kind of procedure. By using this prior information about the type of image that is expected, it is anticipated that a meaningful estimate of the null-space component of the reconstruction will be provided, thereby reducing artifacts. It is essential that the knowledge about the ensemble extend beyond what can be ascertained from an imaging modality that suffers from a limited-data geometry. Otherwise, no information about the null space can be added to the measurements themselves. The Bayesian approach permits prior information about the structure of the reconstructed object to be employed to estimate the null-space components of the solution. Of course, other types of prior information can also be incorporated in the Bayesian method of reconstruction.

Deterministic solutions to the image recovery problem tacitly assume the measurements, Eq. (3.2-3), can be made with infinite accuracy. In reality, all measurements of continuous quantities are subject to random fluctuations called noise. In general, the measurements should be written as

$$\mathbf{g} = \mathbf{H}\mathbf{f} + \mathbf{n}, \tag{3.4-1}$$

where $\mathbf{n}$ is the noise vector. It must be emphasized that the noise vector is a random variable. It is different for each set of measurements and its exact value cannot be correctly guessed. Each realization of the vector $\mathbf{n}$ may be regarded as a random selection from an infinitely large ensemble, or collection, of noise vectors. In general, the noise fluctuations may possess an arbitrary probability density distribution. Frequently, however, the assumption is made that the noise has a multivariate Gaussian distribution with a zero mean

$$\begin{aligned} P(\mathbf{n}) &\sim \exp\{-\tfrac{1}{2}\textstyle\sum n_i[\mathbf{R}_n^{-1}]_{ij}n_j\}, \\ &\sim \exp\{-\tfrac{1}{2}\mathbf{n}^T\mathbf{R}_n^{-1}\mathbf{n}\}, \end{aligned} \tag{3.4-2}$$

where the second expression is in the vector notation of the previous section and $\mathbf{R}_n$ is the noise covariance matrix, the *ij* element of which is

$$[\mathbf{R}_n]_{ij} = \langle n_i n_j \rangle. \tag{3.4-3}$$

The brackets $\langle\,\rangle$ indicate an average over all members of the ensemble of noise vectors. The above expression is general enough to characterize fully noise fluctuations that depend on the strength of the signal being measured or on the position of the measurement, or depend on each other, that is, are correlated. By its definition, $\mathbf{R}_n$ is a positive-definite matrix, and its inverse, needed in Eq. (3.4-2), is assured.

Under a wide range of reasonable conditions [37], when averaged over the full ensembles of noise and images, the best estimate for the reconstruction is that particular image **f** that maximizes the *a posteriori* conditional probability density of **f** given the measurements **g**. This probability is given by Bayes's formula

$$P(\mathbf{f}\,|\,\mathbf{g}) = \frac{P(\mathbf{g}\,|\,\mathbf{f})P(\mathbf{f})}{P(\mathbf{g})} \tag{3.4-4}$$

in terms of the conditional probability of **g** given **f**, $P(\mathbf{g}\,|\,\mathbf{f})$, and the *a priori* probability distributions of **f** and **g** separately, $P(\mathbf{f})$ and $P(\mathbf{g})$.

Herman and Lent [31] and Hunt [38] proposed using the Bayesian approach for image reconstruction. It is assumed that $P(\mathbf{g}\,|\,\mathbf{f})$ is given by $P(\mathbf{n})$, in which **g** is Gaussian distributed about the mean **Hf**, as in Eq. (3.4-2),

$$P(\mathbf{g}\,|\,\mathbf{f}) \sim \exp\{-\tfrac{1}{2}(\mathbf{g} - \mathbf{Hf})^T\mathbf{R}_n^{-1}(\mathbf{g} - \mathbf{Hf})\}. \tag{3.4-5}$$

This may be referred to as the measurement probability density distribution, since it follows solely from the distribution of the error fluctuations in the measurements. This probability is also often called the likelihood function [37]. The *a priori* probability density function for the ensemble of images $P(\mathbf{f})$ is assumed to be a multivariate Gaussian distribution with a mean value $\bar{\mathbf{f}}$ and with a covariance matrix $\mathbf{R}_f$

$$P(\mathbf{f}) \sim \exp\{-\tfrac{1}{2}(\mathbf{f} - \bar{\mathbf{f}})^T\mathbf{R}_f^{-1}(\mathbf{f} - \bar{\mathbf{f}})\}. \tag{3.4-6}$$

Under these assumptions, the maximum *a posteriori* (MAP) solution is easily shown to satisfy [38] the *MAP equation*

$$\mathbf{R}_f^{-1}(\bar{\mathbf{f}} - \mathbf{f}) + \mathbf{H}^T\mathbf{R}_n^{-1}(\mathbf{g} - \mathbf{H}\mathbf{f}) = 0, \tag{3.4-7}$$

where **H** is the linear operator (matrix) corresponding to the projection process described by the integral in Eq. (3.2-1). As shown in the previous section, the transpose of **H** is the familiar backprojection operation. The first term comes from the derivative of $P(\mathbf{f})$ given by Eq. (3.4-6) and the second from $P(\mathbf{g}|\mathbf{f})$, Eq. (3.4-5). It can be seen that the MAP solution strikes a balance between its deviation from the ensemble mean $\bar{\mathbf{f}}$ and the solution to the measurement equation ($\mathbf{g} = \mathbf{H}\mathbf{f}$). This balance is determined by the covariance matrices $\mathbf{R}_f$ and $\mathbf{R}_n$, which specify the confidence with which each deviation is weighted, as well as possible correlations between the deviations. Because the last operation in the second term is $\mathbf{H}^T$, it is only the measurement-space part of this term that has any relation to the first term. It is noted that in Eq. (3.4-7) the linearity in the unknown image **f** follows from the assumption of normal distributions for the *a priori* and measurement-error probability densities.

The MAP reconstruction method presented here is equivalent to the *minimum-variance linear estimator* with nonstationary mean and covariance ensemble characterizations [37]. It is also called the *minimum mean-square-error method* [6]. When the blur function, noise, and ensemble image properties are stationary (do not depend on position), then **H**, $\mathbf{R}_f$, and $\mathbf{R}_n$ are Toeplitz matrices, and, in the circulant approximation, this is the same as the well-known *Wiener filter* [6].

When there is an absence of prior information, as is often the case, the *a priori* probability distribution $P(\mathbf{f})$ does not play a role in Eq. (3.4-4). The MAP approach then reduces to maximizing the conditional probability Eq. (3.4-5) or, what is equivalent, minimizing (−2) times the logarithm of that probability, which is called chi-squared

$$\chi^2 = (\mathbf{g} - \mathbf{H}\mathbf{f})^T\mathbf{R}_n^{-1}(\mathbf{g} - \mathbf{H}\mathbf{f}). \tag{3.4-8}$$

The *minimum chi-squared method*, or the *least-squares method* as it is often called, is a deterministic reconstruction procedure since no reference is made to the stochastic nature of **f**. When **H** is a linear matrix operator, as assumed here, the solution to the χ^2 minimization problem is given in terms of the inverse (or pseudoinverse [33]), Eq. (3.3-4). If the matrix **H** is too large to invert directly, an iterative method might be employed [15, 30, 39]. When **H** is a nonlinear operator, the **f** that minimizes χ^2 can usually be found by an iterative procedure [40]. The minimum χ^2 solution is also often referred to as the *maximum-likelihood solution*, with the probability density distribution given by Eq. (3.4-5) termed the likelihood function [37]. This

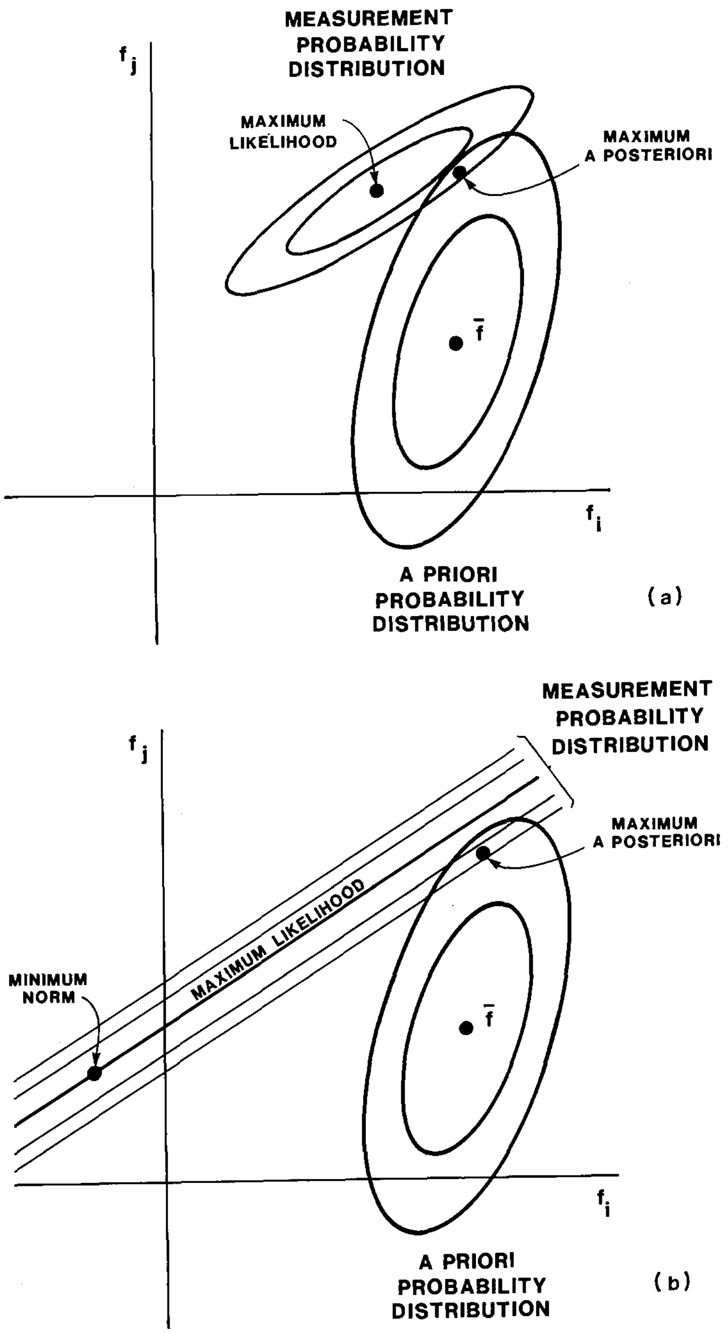
MEASUREMENT PROBABILITY DISTRIBUTION
f_j
MAXIMUM LIKELIHOOD
MAXIMUM A POSTERIORI
$\bar{f}$
f_i
A PRIORI PROBABILITY DISTRIBUTION
(a)
MEASUREMENT PROBABILITY DISTRIBUTION
f_j
MAXIMUM A POSTERIORI
MAXIMUM LIKELIHOOD
MINIMUM NORM
$\bar{f}$
f_i
A PRIORI PROBABILITY DISTRIBUTION
(b)

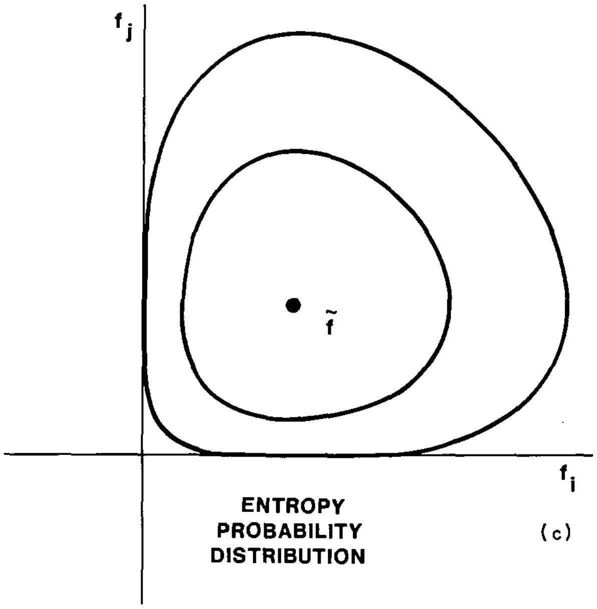

(continued)

usage is not uniformly employed, however [41], as the probability given by Eq. (3.4-4) is sometimes referred to as the likelihood. Reference to maximum likelihood is also legitimate under assumptions about the noise other than it is normally distributed, Eq. (3.4-2). For example, Shepp and Vardi [42] have developed a maximum-likelihood reconstruction algorithm appropriate to Poisson-distributed noise.

The above concepts may be visualized by considering the equal-probability contours in a plane defined by two of the components of the image vector **f**. Figure 3.4-1 shows these contours for a number of situations. Under the assumption of Gaussian probability distributions, the contours

---

Fig. 3.4-1. Contour plots of the probability distributions associated with prior information and the available measurements displayed as a function of two components of the image vector, f_i and f_j, for (a) Gaussian distributions, (b) same with the null space intersecting the f_i-f_j plane, and (c) distribution corresponding to the maximum-entropy principle. In the Bayesian approach, the information provided by the measurements is supplemented by prior knowledge cast in terms of an ensemble mean $\bar{\mathbf{f}}$ and its covariance matrix $\mathbf{R}_f$. The maximum *a posteriori* solution maximizes the product of the *a priori* probability and the measurement probability or likelihood function. Maximum-entropy algorithms may be interpreted in terms of the MAP method with the *a priori* probability distribution replaced by a non-Gaussian distribution specified only by its maximum $\tilde{\mathbf{f}}$. This probability function is nonzero only for positive image values.

are ellipses. The contours for the *a priori* probability distribution are centered on the ensemble mean vector $\bar{\mathbf{f}}$ and their shape and extent is controlled by the *ii*, *jj*, and *ij* elements of $\mathbf{R}_f$. The contours for the *a posteriori* distribution are centered on the deterministic maximum-likelihood (least-squares) solution. Their shape is affected by the noise covariance matrix $\mathbf{R}_n$ and the measurement matrix $\mathbf{H}$. If the f_i-f_j plane includes a component of the null space, there is no unique solution for f_i and f_j that satisfies the measurements Eq. (3.2-3). Figure 3.4-1b represents such a situation. Every point on the solution line of Fig. 3.4-1b yields exactly the same measurement vector. Deterministic algorithms based on the minimum-norm criterion select the point on the solution line that is closest to the origin. The MAP approach leads to a solution that is closer to the ensemble mean value in this plane, ignoring off-diagonal correlations in $\mathbf{R}_f$. The relationship between MAP and the maximum-entropy approach will be considered in the next section.

When the solution to the above MAP equation is averaged over the complete ensemble of noise and images, and the correct values are used for the *a priori* entities, the resulting $\langle \mathbf{f} \rangle$ can be shown to be *unbiased*; that is, it is the same as $\bar{\mathbf{f}}$ [37]. However, if the wrong $\bar{\mathbf{f}}$ is used and $\mathbf{R}_f^{-1}$ is nonzero, then $\langle \mathbf{f} \rangle$ will be biased. Of more importance is the fact that for subensembles of images whose mean characteristics are different from those of the ensemble, the MAP estimates are biased toward the ensemble mean. This is an important consideration when the objective of the imaging and reconstruction task is to identify abnormal occurrences, as in looking for diseased hearts. If the ensemble contains a preponderance of normal individuals, the abnormals will tend to be made to appear as normal by the MAP algorithm. This sort of consideration may require us to return to the fundamental statement of MAP and change the cost function to reflect the fact that a misidentified abnormal may be less acceptable than a misidentified normal (as in heart diagnosis). Alternatively, one might allow for greater deviations from $\bar{\mathbf{f}}$ than the true ensemble value of $\mathbf{R}_f$ indicates.

3.5 USE OF OTHER KINDS OF PRIOR KNOWLEDGE

One of the main features of the MAP approach presented in the previous section is that it provides a method of supplementing the available measurements with information previously known about the shape or structure of the reconstructed object. Various other extensions to deterministic algorithms have been proposed to improve the reconstructions from limited data through the use of *a priori* knowledge about the object. These include consistency, analytic continuation, region of support, upper and lower limits, and maximum entropy, which will be discussed in turn. The Bayesian approach may be argued to encompass all of these in one way or another.

Inouye [43] used the consistency between the measurements that is implied by the statement that all are projections of a single 2-D object. Inouye expressed this consistency through the allowed functional forms of the moments of the projections. Of course, consistency is inherent in any reconstruction algorithm that satisfies the measurement equations Eq. (3.2-1). Inouye [44] also advanced a method of calculating the missing views that is based on the Tschebyscheff polynomial expansion originally used by the CT vanguard, Allan Cormack [45]. This method is closely related to analytic continuation. Hanson [24] concluded that these proposed methods of coping with missing data are ineffective in overcoming the measurement-space restrictions presented above for the solution of the general problem.

Tam *et al.* [46] introduced a method to use the *a priori* known region of support of the source distribution. This method is the 2-D counterpart of the celebrated *Gerchberg–Papoulis algorithm* [47, 48] for obtaining "*super-resolution.*" It is an iterative technique in which the known properties of the image in the spatial and Fourier domains are alternatively invoked. The objective is to use the known spatial extent of the source to extend the 2-D Fourier transform of the reconstruction from the "known" sector into the "missing" sector (Section 3.2 and Chapter 9). This method has been studied extensively [49–52] and has been shown to have some merit when either the region of support is very restrictive or the angular region of the missing projections is fairly narrow. Tam and Perez-Mendez analyzed this problem by evaluating the eigenfunction map of the matrix that is the product of the constraints of a circular region of support and band-limitedness.

It is known to be possible to completely determine an integrable function with a finite domain of support from projections that are continuous in angle over some finite range and have infinite spatial resolution [7, 44]. Thus, the null space must be empty and the eigenvalues in the analysis of Tam and Perez-Mendez must not actually go to zero in the limit of an infinite number of angles. The function to be reconstructed must be representable by the response-function expansion. This seems at odds with the interpretation of the limited-angle CT problem as one of a missing sector in the 2-D Fourier domain. However, the projection-slice theorem holds only for projections over the infinite plane. When the object is restricted to a finite domain, the Fourier transform of each parallel projection set, although being concentrated along the slice, actually has infinite extent perpendicular to the slice. Thus, the projections of an object with known finite region of support do sample the missing sector. The above theorem may then be interpreted as saying that when there is an infinite number of samples from that sector, the Fourier amplitudes in the sector may be recovered because the totality of response functions provides a complete basis for the full 2-D frequency domain. The missing sector is not missing at all! Incidentally, the problem of superresolution may be similarly approached from the standpoint of a measurement-space expansion. The Gerchberg–Papoulis algorithm has been shown to be a special case of a general SIRT-like iterative procedure due to Bialy [15].

The region-of-support constraint may be incorporated more directly into many reconstruction algorithms. In virtually every iterative algorithm it is possible to invoke constraints on the reconstructed function by restricting the function as part of the updating step. Such iterative algorithms yield a solution that satisfies the region-of-support constraint, and Tam's procedure is not required. This constraint may be enforced through a redefinition of the response functions $h_i(x, y)$ in Eq. (3.2-1) to make them zero outside the region of support. Then the backprojection operation, Eq. (3.3-1), only affects the reconstruction within the region of support. With this redefinition of the $h_i(x, y)$, the measurement space includes only functions that fulfill the region-of-support constraint. From this standpoint, Tam's iterative procedure does not affect the null space associated with the available measurements. The natural-pixel formulation of Buonocore *et al.* [25, 53] may be revised in a similar manner, but that would probably ruin the properties of the measurement matrix they exploited to arrive at an efficient matrix calculation.

Often it is known that the physical quantity to be reconstructed cannot be negative, as, for example, light intensity, density, pressure, and linear attenuation coefficients. Thus, it has been suggested by numerous authors that reconstructions of such quantities should be constrained to be nonnegative—Gordon *et al.* [16], Huang *et al.* [54], Herman and Lent [39], Schafer *et al.* [55], Sezan and Stark [56], and Medoff *et al.* [22], to name just a few. A simple extension of this is the constraint of known upper and lower limits on the reconstruction function. Imposition of such constraints can be very effective when a major portion of the image is close to the limits. Likely candidates are renditions of text and photographs of the heavens. For this kind of image, the limits are likely to be violated by artifacts and noise. Thus, by invoking bounds on the reconstructed function, these transgressions would be reduced and the final image is likely to be more pleasing. The value of the lower-bound constraint in overcoming the difficulties associated with the null space can be inferred from the excellent maximum-entropy reconstruction of text shown in Burch *et al.* [57] and was explicitly demonstrated by Trussell and Civanlar [58]. Hanson [59] has found that in favorable circumstances, the nonnegativity constraint can improve the visualization of objects when it is hindered by either artifacts produced by the limited nature of the data or noise in the measurements. When most of the image values are far removed from legitimate limits, as in CT scans of the brain, the use of such limits cannot be expected to change the results.

Figure 3.4-1 brings to mind the concepts presented in Chapters 2, 8, and 11 having to do with *projections onto convex sets* (POCS) [56, 60]. This correspondence is valid if one restricts oneself to the set of solutions possessing prior or measurement probabilities greater than a fixed value. For the measurement probability distribution, this amounts to placing a bound on χ^2. Then the sets have well-defined boundaries. Furthermore, for multivariate Gaussian probability distributions, the sets are obviously convex. Of course, one of the great advantages of the POCS method is that it permits the use of numerous constraints that are beneficial in image restoration [56, 58] but cannot be easily incorporated in conventional algorithms. One disadvantage of the POCS method is that it yields only one solution out of a possibly infinite set of feasible ones if the sets overlap substantially. Furthermore, the POCS solution in this case depends on the starting point and on the ordering of the projection operations. Trussell and Civanlar [61] have used the POCS approach to solve the MAP problem with several side constraints by varying the probability level that defines the boundaries of the sets until the MAP equation is satisfied. In its full generality, however, the Bayesian approach is not restricted to this kind of arbitrary threshold in probability. Because the probability values are often continuous, the sets involved in the Bayesian analysis are fuzzy.

Many authors have proposed and used the *maximum-entropy* condition to ameliorate artifacts in reconstructions. For examples, see Chapter 5 as well as Frieden [41], Wernecke and d'Addario [62], Gull and Daniell [63], and Minerbo [64]. In the straightforward approach, it is desired to find the solution to the measurement equations, Eq. (3.2-1), that maximizes the entropy

$$S = -\sum p_i \ln(p_i), \tag{3.5-1}$$

where p_i is the portion of the total intensity that lies in the ith pixel

$$p_i = f_i / \sum f_i. \tag{3.5-2}$$

It is assumed that $p_i \geqslant 0$. Andrews and Hunt [6] and Minerbo [64] showed by means of the method of Lagrange multipliers that, when the sum of f_i is considered to be a constant, the maximum-entropy condition leads to a solution of the form

$$\ln\{\hat{f}(x, y)\} = C + \sum_{i=1}^{N} \lambda_i h_i(x, y), \tag{3.5-3}$$

where C is an additive constant and the λ_i are the Lagrange multipliers, which must be adjusted to satisfy the measurement equations. The maximum-entropy principle implies a solution whose logarithm is proportional to an expansion in terms of response functions, in much the same way as the minimum-norm condition yields the linear, response-function expansion form, Eq. (3.3-1). Equation (3.5-3) enforces the nonnegativity constraint inherent in maximum entropy.

Recognizing the fundamental difficulty of this approach when the data are inconsistent, that is, when no solution to Eq. (3.2-3) exists, Gull and Daniell [63] merged maximum entropy with the probabilistic concepts of random noise by proposing that one find the solution that maximizes entropy subject to the constraint that χ^2 be equal to a predetermined value x_0^2. Andrews and Hunt [6] suggested this as an alternative form of the constrained least-squares approach but did not show any results. The resulting expression for the quantity to be minimized appears very similar to the quadratic form of the logarithm of the *a posteriori* probability function based on Gaussian probability distributions, Eqs. (3.4-5) and (3.4-6), that led to the standard MAP equation (3.4-7). The similarity prompts one to interpret the maximum-entropy technique in terms of a Bayesian approach [65] in which the *a priori* probability density is given by

$$[(\mathbf{f}) \sim \exp\left\{-N \sum_i f_i \ln\left(\frac{f_i}{e\tilde{f}_i}\right)\right\}. \tag{3.5-4}$$

The constant e is required for normalization purposes to make the maximum of $P(\mathbf{f})$ coincide with the vector $\tilde{\mathbf{f}}$, which takes the place of the ensemble mean $\bar{\mathbf{f}}$ in Eq. (3.4-6) [57]. The constant N is the number of something—photons in the image, or pixels, or balls thrown by monkeys, or whatnot. Its interpretation is still being studied [66]. In any event, the value of N is computationally considered to be a Lagrange multiplier that is varied to bring χ^2 to the required value [57]. Independent of whether this Bayesian interpretation is correct or not, the performance of the maximum-entropy algorithm can be understood and interpreted in terms of what one expects for MAP under the assumption of a prior probability distribution given by Eq. (3.5-4). The contours of this probability distribution given by Eq. (3.5-4). The contours of this probability distribution are shown in Fig. 3.4-1c with $\tilde{\mathbf{f}}_i = \tilde{\mathbf{f}}_j = 0.0001$ and $N = 10{,}000$. It is observed that this entropy probability function is quite broad. Near its maximum $\tilde{\mathbf{f}}_i$, its behavior is similar to that of a Gaussian with an rms width of about $\tilde{\mathbf{f}}_i$. Thus, the conventional MAP approach, augmented to include a constraint of nonnegativity, might be expected to yield results quite similar to those obtained with a maximum-entropy algorithm. This has been our experience, as shown in Fig. 3.10-1, referred to in Section 3.10. As N gets smaller, the above probability distribution becomes even flatter.

The above interpretation of the maximum-entropy algorithms in terms of the Bayesian probabilistic philosophy is contrary to the axiomatic approach to maximum entropy espoused by many [66, 67]. Some would prefer to view MAP as a special case of the maximum-entropy principle [68]. However, others find it difficult to accept the interpretation of image intensities as probabilities [69]. To add to the confusion, the proper choice for the entropy expression has been a constant source of debate [70, 71]. One advantage of the Bayesian interpretation is that it permits one to ask whether the entropy probability distribution Eq. (3.5-4) represents an appropriate *a priori* probability distribution for the particular problem one is addressing.

3.6 MAP SOLUTIONS

We have adopted an iterative approach to the solution of Eq. (3.4-7) based on the scheme proposed by Herman and Lent [31]. The iteration scheme is given by

$$\mathbf{f}^0 = \bar{\mathbf{f}}, \tag{3.6-1a}$$

$$\mathbf{f}^{k+1} = \mathbf{f}^k + c^k \mathbf{r}^k, \tag{3.6-1b}$$

$$\mathbf{r}^k = \bar{\mathbf{f}} - \mathbf{f}^k + \mathbf{R}_f \mathbf{H}^T \mathbf{R}_n^{-1}(\mathbf{g} - \mathbf{H}\mathbf{f}^k), \tag{3.6-1c}$$

$$c^k = \mathbf{r}^{kT}\mathbf{s}^k / \mathbf{s}^{kT}\mathbf{s}^k, \tag{3.6-1d}$$

$$\mathbf{s}^k = (\mathbf{I} + \mathbf{R}_f \mathbf{H}^T \mathbf{R}_n^{-1}\mathbf{H})\mathbf{r}^k, \tag{3.6-1e}$$

where vector $\mathbf{r}^k$ is the residual of Eq. (3.4-7) (multiplied by $\mathbf{R}_f$), the scalar c^k is chosen to minimize the norm of $\mathbf{r}^{k+1}$, and $\mathbf{I}$ is the identity matrix. When the residual goes to zero, the corresponding $\mathbf{f}^k$ is clearly a solution of the MAP Eq. (3.4-7). This iterative scheme is very similar to the one proposed by Hunt [38] for MAP image restoration in the presence of a nonlinear scalar transfer function. His update scheme consisted in incrementing $\mathbf{f}^k$ by Eq. (3.6-1c) multiplied by $\mathbf{R}_f^{-1}$. This might introduce computational difficulty if $\mathbf{R}_f$ is nontrivial. Trussell and Hunt [72] refined Hunt's iteration procedure to improve the rate of convergence. We have found that Eq. (3.6-1) works well, although convergence typically requires 10 to 20 iterations. An advantage of any iterative reconstruction scheme is that constraints may readily be placed on the reconstructed function $\mathbf{f}^{k+1}$ after each update. Such constraints include upper and lower limits to the reconstruction value, known region of support, etc. The reconstruction algorithm can thus become quite nonlinear.

It is easy to see from the form of this iterative procedure that significant null-space contributions to $\mathbf{f}^k$ can arise from the *a priori* information. First, the zero-order estimate is $\bar{\mathbf{f}}$, which can contain nill-space contributions. Second, in Eq. (3.6-1c), $\mathbf{R}_f$ can generate null-space contributions when it operates on the result of the backprojection ($\mathbf{H}^T$) process, which lies wholly in the measurement space. In effect, $\mathbf{R}_f$ weights the backprojection of the measurement residuals. If $\mathbf{R}_f$ is chosen to be zero in certain regions of the reconstruction, these regions will not be altered from $\bar{\mathbf{f}}$ throughout the iteration scheme. Prior structural information about the source function can be incorporated in both $\bar{\mathbf{f}}$ and $\mathbf{R}_f$. It must be emphasized that the choices for $\bar{\mathbf{f}}$ and $\mathbf{R}_f$ are crucially important because it is only through them that a nonzero null-space contribution to the reconstruction arises. As stated earlier, this is the major advantage of the Bayesian approach over deterministic algorithms. Trivial choices, such as using for $\bar{\mathbf{f}}$ a constant or a filtered backprojection reconstruction based on the same projections, or assuming $\mathbf{R}_f$ to be proportional to the identity matrix [38, 73], are not helpful for reducing artifacts because they do not affect the null-space components of the solution. However, it has been shown that noise amplification in nearly singular inversions, as in Abel inversion [74], can be controlled through the choice of a smoothed value of $\hat{\mathbf{f}}$ for $\bar{\mathbf{f}}$ and a diagonal smoothing matrix for $\mathbf{R}_f$ [75]. With these choices the MAP algorithm is similar to one form of the constrained least-squares method [6]. By reducing extremely large noise fluctuations, the result can be made more acceptable to the eye [76].

The iteration scheme given by Eq. (3.6-1) is *SIRT-like* [31], which means that the reconstruction update, Eq. (3.6-1b), is accomplished only after all the ray sums ($\mathbf{Hf}^k$) have been calculated. It is known that *ART-like* algorithms converge much faster than SIRT-like ones [26, 39]. ART-like algorithms originated with Kaczmarz [77]. They are based on an iteration scheme in which each measurement is calculated from the present estimate of $\mathbf{f}$ using the corresponding row of the matrix $\mathbf{H}$. The difference between that and the actual measurement is redistributed among the contributing components of $\mathbf{f}$ by means of backprojection with the proper normalization to assure agreement. Tanabe [11] showed that this is a fast algorithm for finding the generalized inverse of a matrix. Iterative algorithms of this sort have been proposed for restoring blurred images with nonlinear constraints [54]. Trussell and Civanlar [78] have pointed out the relationship ART and SIRT have to the method of projection onto convex sets, which is presented in Chapters 2, 8, and 11. Herman *et al.* [73] have proposed an ART-like reconstruction algorithm that converges to the solution of the MAP equation, Eq. (3.4-7), under the assumption that $\mathbf{R}_f$ and $\mathbf{R}_n$ are proportional to the identity matrix. This algorithm is worth exploring as it may converge much more rapidly than the one used here. However, as stated above, this algorithm should be extended to include nontrivial choices for $\mathbf{R}_f$. The iterative scheme used here, although it may be slower than necessary, does provide a solution to the MAP equation, which is the important thing for demonstrating the usefulness of the Bayesian method. The present algorithm converges such that the norm of the residual, Eq. (3.6-1c), behaves as the iteration number raised to the -1.5 to -2.0 power.

It is well known that the assumption of normal probability density distributions leads to a MAP solution, Eq. (3.4-7), that is equivalent to the minimum-variance linear estimator [37]. This estimator has been applied in a matrix formalism to tomographic reconstruction by Wood *et al.* [79, 80] and Buonocore *et al.* [53]. These authors stressed the importance of *a priori* information in limited-angle reconstruction. The main thrust of their work was toward improving the computational efficiency of the required matrix operations, in which they were very successful. However, simplifying assumptions about the geometry of the measurements or about the ensemble coefficients had to be made in order to develop efficient methods. Even though the general MAP equation may be solved by direct matrix methods, the size of the matrices involved is typically too large to deal with on present-day computers. Also, it is difficult to add nonlinear constraints such as upper or lower limits to the reconstruction. The above iterative method of solution overcomes these difficulties.

Recently, Smith *et al.* [81, 82] introduced a new method of image reconstruction called *simulated annealing*, which Geman and Geman [83] have shown can be used to obtain MAP solutions. This method is akin to Monte Carlo procedures for multidimensional integration in that the updaate scheme used is stochastic. It is based on a physical interpretation of the above probability distributions in terms of energies associated with a system of statistical mechanical particles. The state of randomly selected pixels is queried and adjusted according to the total energy and the temperature of the system through a random sampling from a Gibbs probability distribution. After beginning with the system at a high temperature, the temperature is gradually lowered. This annealing process ultimately brings the system to its lowest-energy state, which is the desired solution. The power of this method is that the energy functions employed can reflect prior knowledge about complicated structure. Because there is no smooth progression from the initial state to the final one, as there is in the standard MAP and POCS techniques, it is not necessary to restrict oneself to constraint sets that are convex. In their examples, Geman and Geman chose energy functions that maximized the probability for smooth reconstructions. They augmented this with a "line process" that allowed breaks in the smooth reconstruction along lines. Their final reconstructions closely followed the input images, which consisted of a mosaic of irregularly shaped regions of nearly constant intensity. Certain kinds of constraints, such as region of support and nonnegativity, can also be incorporated in this algorithm in the form of hard constraints [84]. Thus simulated annealing offers an appealing alternative way to incorporate certain kinds of prior knowledge about the structure of the reconstructed object that may be difficult to implement in and may depart drastically from the simplifying assumptions of the standard MAP method. This method would appear to be most easily computed when the energy functions involve a small number of pixels.

3.7 FAIR—FIT AND ITERATIVE RECONSTRUCTION

The fit and iterative reconstruction technique introduced by Hanson [85] offers an alternative method for incorporating *a priori* information about the source function is used to construct a parametric model of the unknown function. What is known about the structure of the object is employed to restrict the structure of the model. The first step in this algorithm is to determine the parameters in the model from the available projection data by a least-squares [or minimum chi-squared, Eq. (3.4-8)] fitting procedure. In the second step of FAIR, an iterative reconstruction procedure is performed, using the fitted parametric model as the initial estimate. The iterative reconstruction procedure forces the result to agree with the measurements through alteration of its measurement-space contribution. The null-space contribution to the FAIR reconstruction arises solely from the parametric model fitted in the first step and hence from the *a priori* information used in specifying the model. In a certain sense, this parameter estimation problem may be viewed as a selection of that point in Hilbert space which satisfies the constraints placed on the function through specification of the parametric model and minimizes chi-squared. Although the ART algorithm [16] has been used in the second, iterative step of FAIR, other iterative algorithms such as the MAP algorithm above can be used advantageously (see Section 3.6). It might be noted that ART, as usually employed, forces the reconstruction to agree with each measurement in turn and is unable to accommodate inconsistent data (contaminated by noise, for example). However, when employed with a vanishingly small damping factor, or relaxation parameter, ART can cope with inconsistent data and will converge to a least-squares solution [86].

An important advantage of using the fitting procedure in the FAIR technique is its flexibility. Additional parameters may be introduced in the model to permit the position, orientation, and size of the object to be adjusted to match the data. Constraints may be placed on the extra parameters to avoid unacceptable objects. For example, in the annulus problems below, it is possible to allow each of the 2-D Gaussian functions to be centered at a variable radius instead of a fixed, predetermined radius. This would permit the size and the shape of the contour of the annulus to be determined from the measurements. The anular structure of the modeled object could still be enforced by adding a penalty function to chi-squared based on the quadratic differences between the radii of adjacent Gaussians. This MAP approach to parameter estimation would tend to make the radius a smooth function of polar angle.

3.8 COMPARISON OF MAP AND FAIR RESULTS

The results of application of various reconstruction methods to a specific two-dimensional, limited-angle reconstruction problem will be compared. Algorithms that are useful for handling incomplete data through the use of *a priori* information must have the following important characteristics. They must (1) significantly reduce artifacts that result from inappropriate null-space contributions, (2) gracefully respond to inconsistencies between the actual source function and the assumptions about it, and (3) tolerate noise in the projection data. It will be demonstrated that the MAP and FAIR algorithms conform to these requirements.

These reconstruction techniques have been applied to a source function consisting of a fuzzy annulus with variable amplitude, Fig. 3.8-1a, which roughly emulates the nuclear isotope distribution in the cross section of a heart [87]. The peak value of the distribution is 1.24. The available projection data consist of 11 views covering 90° in projection angle. At first no noise was added to the projections. Each projection contained 128 samples evenly spaced over the full width of the image. All reconstructions contain 128 × 128 pixels. The mean diameter of the annulus is 64 pixels. The measurement-space reconstruction obtained with ART [16], Fig. 3.8-1b, shows severe artifacts that tend to obscure much of the source distribution.

Figure 3.8-1c shows the reconstruction obtained with the maximum-entropy algorithm MENT provided to us by Minerbo [64]. This algorithm provides a modest improvement over ART, particularly in regard to the detection of the dip in the annulus at 50°. However, MENT does not have much effect on the splaying of the reconstruction along the central axis of the available views. In our experience the principal advantage of the maximum-entropy constraint appears to be its implicit constraint of nonnegativity. ART reconstructions that are constrained to be nonnegative are

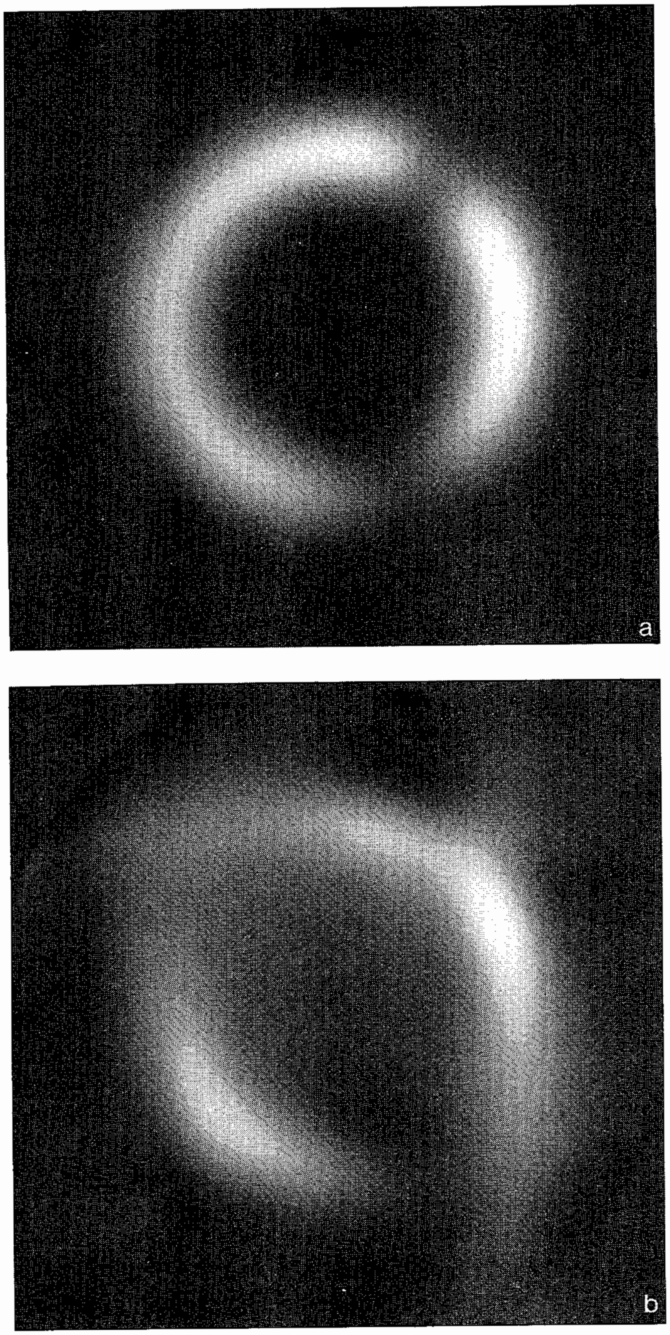
a
b

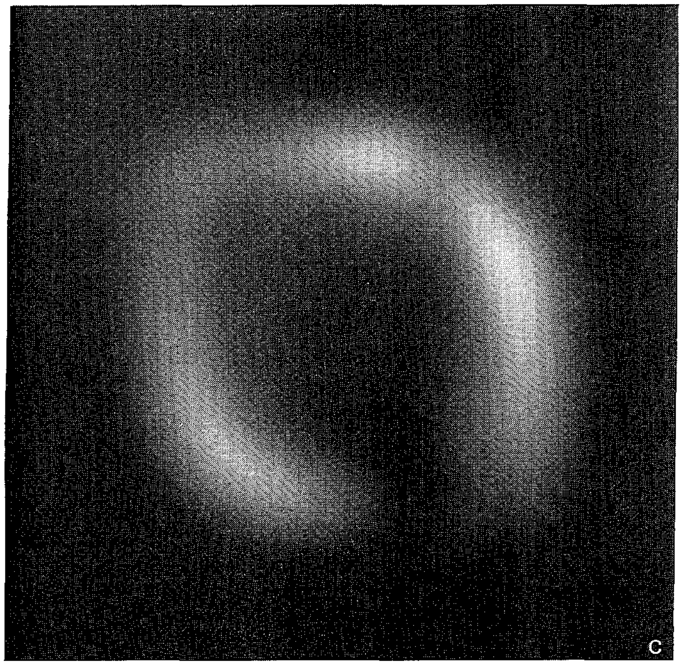

(*continued*)

very similar to the MENT results [85]. The nonnegativity constraint amounts to the incorporation of *a priori* knowledge about the source function. This constraint is generally applicable and is very effective in the reconstruction of certain types of source distributions, such as pointlike objects on a zero background. However, there are many source distributions and data collection geometries for which nonnegativity provides little benefit, such as the present test case. We will not apply the nonnegativity constraint in the remainder of these comparisons to emphasize the value of using *a priori* knowledge about the shape of the object.

It was assumed that the *a priori* information consisted of the knowledge that the source function had an annular structure with known position, radius, and width. Thus, in the MAP approach, $\bar{\mathbf{f}}$ was chosen to be an annulus with constant amplitude and Gaussian cross section. The mean radius and width of the annulus were chosen to be the same as the unknown source function. The covariance matrix $\mathbf{R}_f$ was assumed to be diagonal and thus could be represented as an image proportional to the ensemble variance about the mean $\bar{\mathbf{f}}$. The covariance image $\mathbf{R}_f$ was large (1.0) at the peak of

Fig. 3.8-1. (a) Source distribution used for the first example. (b) ART and (c) MENT reconstructions obtained using 11 views covering 90° in projection angle. Unconstrained ART was used, while MENT has an implicit nonnegativity constraint.

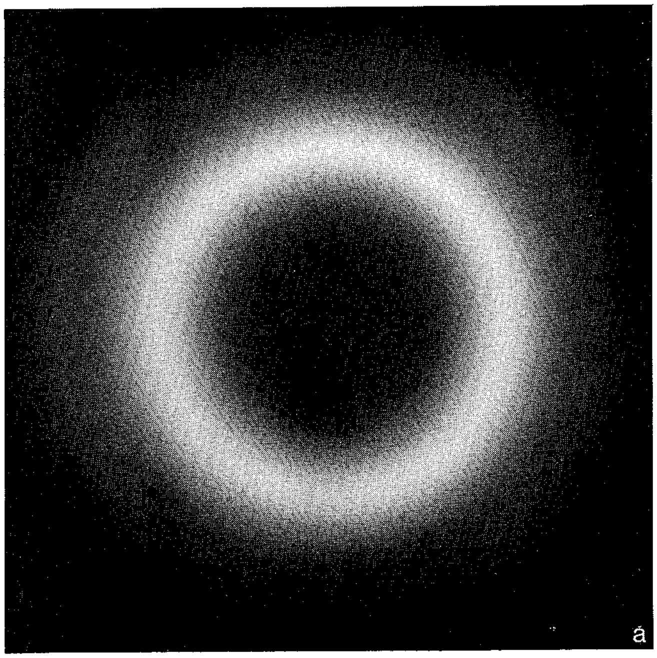
a

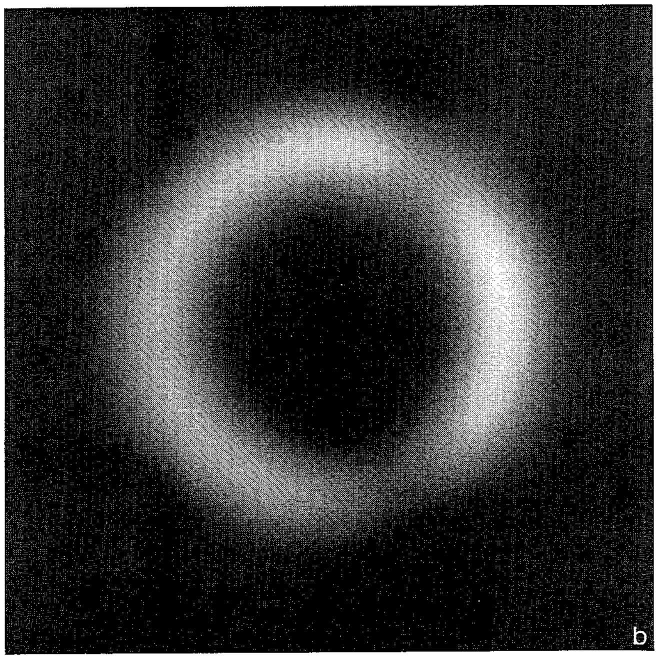
b

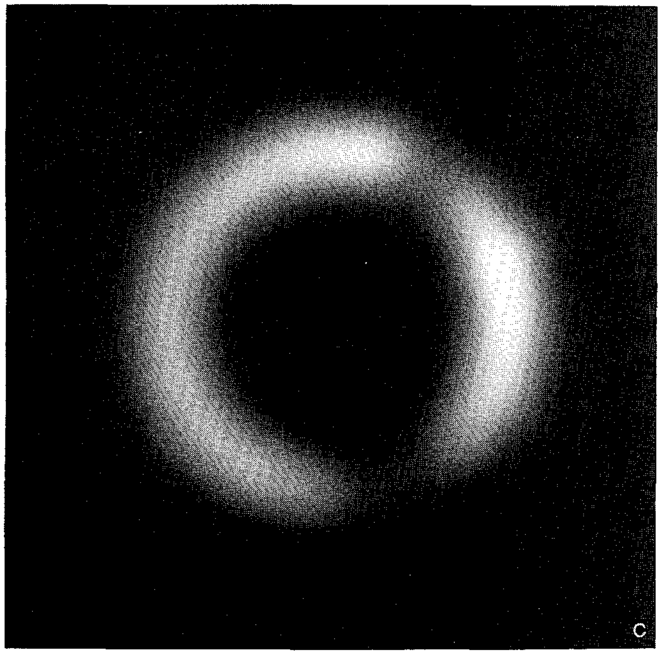

(*continued*)

the annulus and small (0.2) inside and outside, Fig. 3.8-2a. Because noiseless projections were used, the measurement noise was assumed to be uncorrelated, constant, and low in value. The resulting MAP reconstruction, Fig. 3.8-2b, is vastly superior to the ART and MENT results, eliminating essentially all the artifacts present in these deterministic solutions. The parametric model chosen for the FAIR method consisted of 18 two-dimensional Gaussian functions evenly distributed on a circle. The radius of the circle and the width of the Gaussians were chosen to be the same as those of the source function. The fitting procedure determined the amplitude of each of the Gaussian functions. The resulting fitted function was used as the initial estimate in ART to obtain the final result, Fig. 3.8-2c. This FAIR reconstruction is comparable to the MAP result.

Fig. 3.8-2. Reconstructions obtained by using the *a priori* information that the unknown source function is a fuzzy annulus with known radius and width. The MAP reconstruction (b) was obtained with a flat annulus for the ensemble mean $\bar{\mathbf{f}}$, and the variance image (a) as the diagonal entries of the ensemble covariance matrix $\mathbf{R}_f$ (nondiagonal entries assumed to be zero). The FAIR result (c) was based on a model of the image consisting of 18 Gaussian functions distributed around the circle. The use of *a priori* knowledge significantly reduces the artifacts present in the deterministic reconstruction in Fig. 3.8-1.

For a quantitative comparison, Fig. 3.8-3 shows the maximum reconstruction value obtained along radii as a function of angle for the various reconstruction methods presented in Figs. 3.8-1 and 3.8-2. The FAIR reconstruction is seen to follow the original source dependence most closely, with the MAP result a close second. The ART reconstruction has many quantitatively serious defects. The computation times on a CDC-7600 for the algorithms presented here are ART (10 iterations), 17 s; MAP (10 iterations), 73 s; FAIR (3 iterations), 25 s; MENT (6 iterations), 105 s. The corresponding execution time for filtered backprojection is 5 s.

A slightly different source function, Fig. 3.8-4a, was used to test the ability of the algorithms to deal with inconsistencies between assumptions about the source function and its actual distribution. This source function is the same as Fig. 3.8-1a with a narrow, 0.6 amplitude, 2-D Gaussian added outside the annulus at 330° and a broad, 0.1 amplitude, Gaussian added

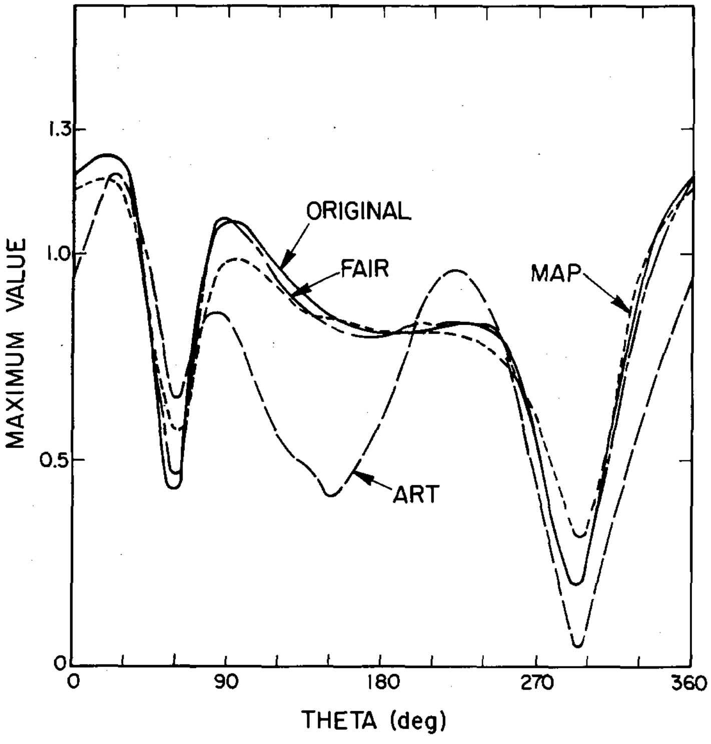

Fig. 3.8-3. Angular dependence of the maximum values along various radii for the ART, MAP, and FAIR reconstructions in Figs. 3.8-1 and 3.8-2 compared with that for the original function, Fig. 3.8-1a, quantitatively demonstrating the improvement afforded by MAP and FAIR.

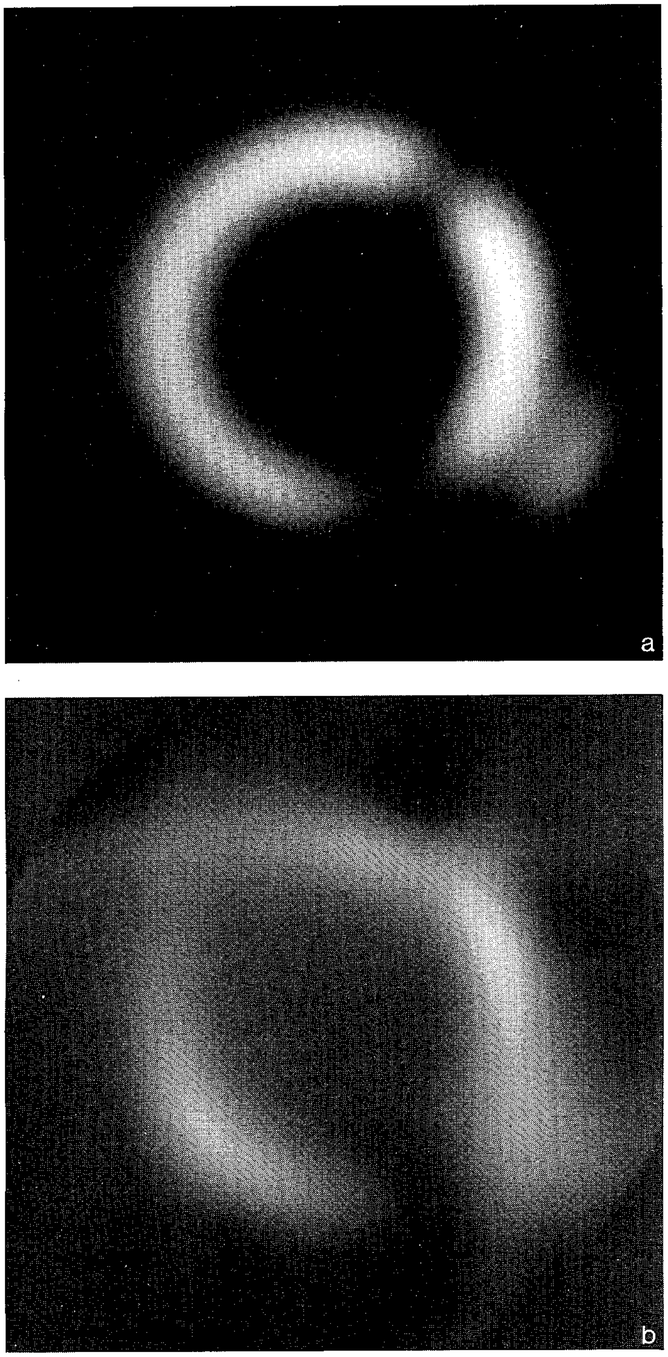
a
b

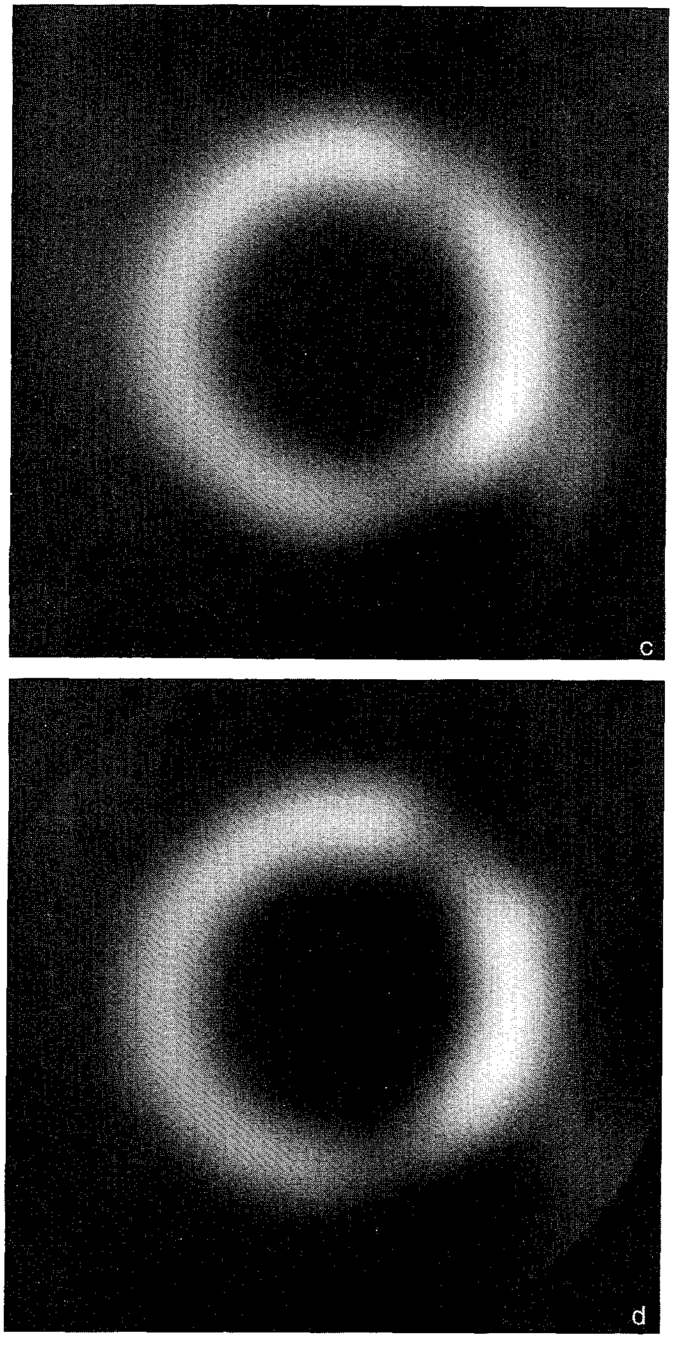

Fig. 3.8-4. Reconstructions of a source distribution (a) that does not conform to the annular assumption obtained from 11 views subtending 90° with the (b) ART, (c) MAP, and (d) FAIR algorithms. Both MAP and FAIR tend to move the additional source placed outside the annulus onto the annulus. However, they provide indications in the reconstructions that there is some exterior activity.

underneath the annulus at 162°. The reconstructions obtained using the same assumptions as above are shown in Figs. 3.8-4b to 3.8-4d. Both MAP and FAIR handle the inconsistencies similarly. The angular dependence of the maximum reconstruction value, Fig. 3.8-5, shows that both algorithms produce an excess near 330° since they tend to shift the discrepant exterior source to the annulus, consistent with the *a priori* assumptions. However, both methods do have a significant response in the region of the exterior source and, therefore, provide some information about the discrepancy. This would not be the case for the MAP algorithm were $\mathbf{R}_f$ chosen to be zero outside the annulus. This illustrates the need for conservatism in placing restrictions on the reconstructions that may be violated by the actual source distribution. The second, iterative reconstruction step in the FAIR method is needed for the same reason as it allows corrections to be made to the fitted model, if indicated by the available projections.

The final example is the reconstruction of Fig. 3.8-1a from noisy data. The same 11 projections were used as before but with random noise added,

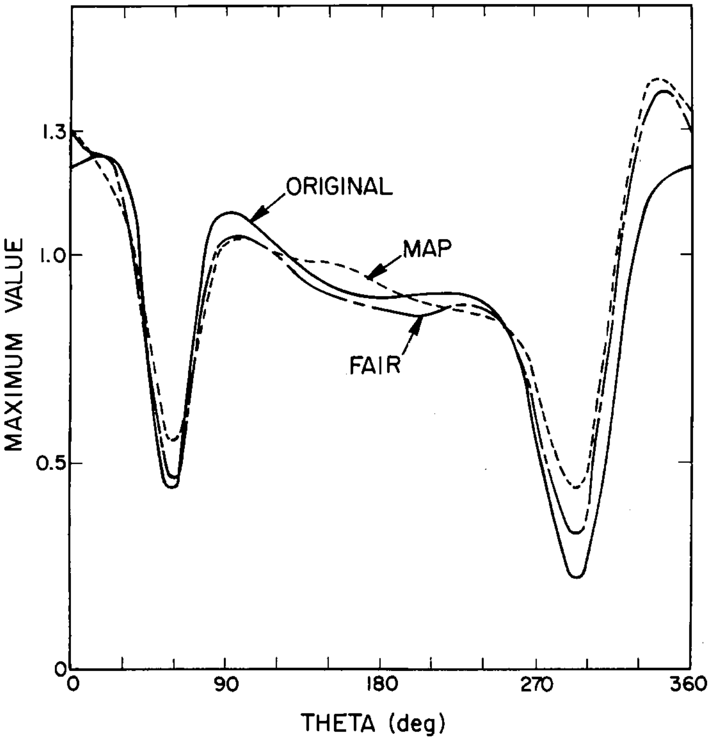

Fig. 3.8-5. Angular dependence of the maximum values in the MAP and FAIR reconstructions of Fig. 3.8-4.

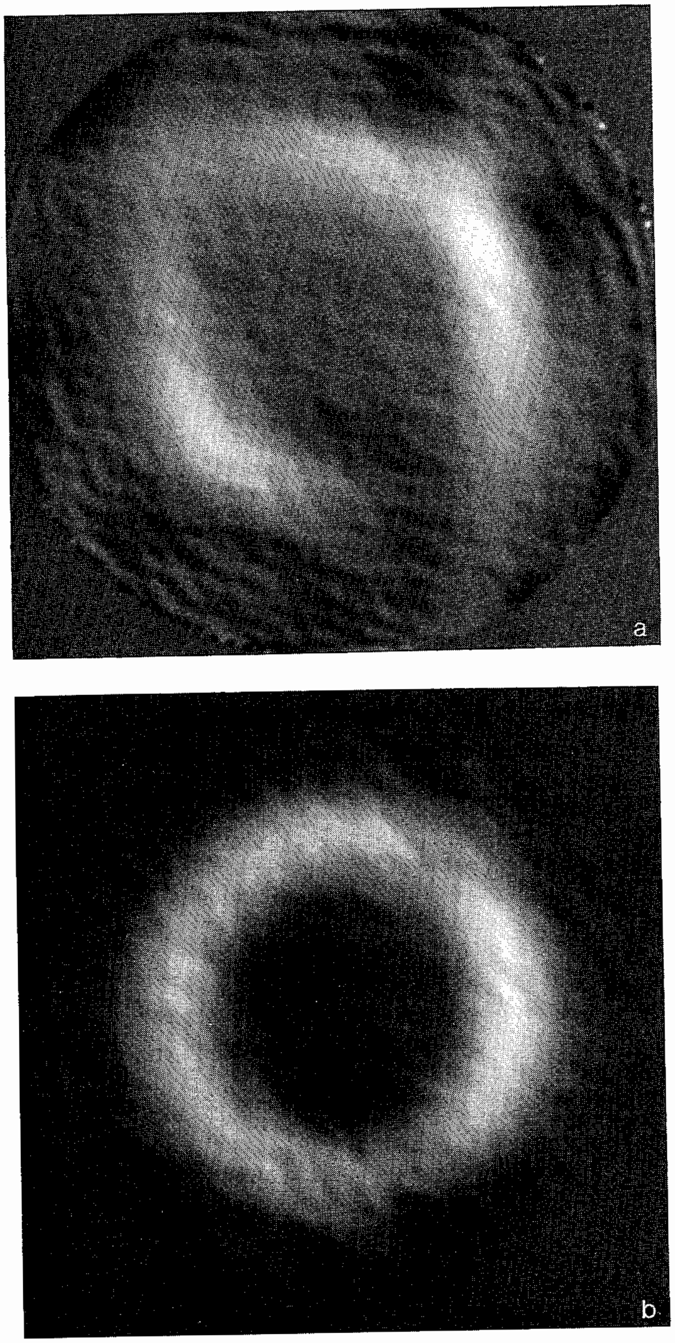
a
b

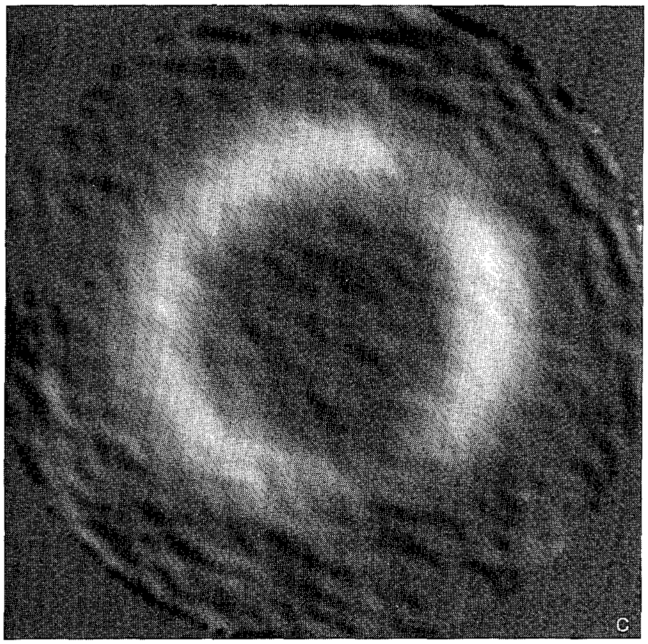

(*continued*)

which has an rms deviation of 10% relative to the maximum projection value. The reconstructions in Fig. 3.8-6 demonstrate that both MAP and FAIR simply yield noisy versions of those obtained from noiseless projections. There is no disastrous degradation as would be expected for algorithms based on analytic continuation [43, 44]. Although the FAIR result appears to be much noisier than the MAP reconstruction, careful observation reveals that both have nearly identical noise in the annular region, which is the only region of interest for diagnosis. The rms difference between the projection measurements and the ray sums of the MAP and FAIR reconstructions, respectively, are roughtly 0.8 and 0.5 times the actual rms deviation of the noise in the projections. This indicates that both algorithms have attempted to solve the measurement equations beyond what is reasonable. The MAP algorithm does balance the rms error in the projections against the deviation from $\bar{\mathbf{f}}$. However, when used with unity damping factor, ART simply attempts to reduce the rms projection error to zero, satisfying each projection

---

Fig. 3.8-6. Reconstructions of the source in Fig. 3.8-1a from 11 noisy projections with the (a) ART, (b) MAP, and (c) FAIR algorithms, showing that the latter two algorithms are tolerant of noise.

in turn. It may never converge to a solution if the data are inconsistent. It is possible to temper the adverse reaction of ART to inconsistent data by using small damping factors [86].

3.9 A GENERALIZED BAYESIAN METHOD

Both MAP and FAIR, as presented above, have drawbacks. The incorporation of *a priori* knowledge in the MAP algorithm presented above is quite restrictive. It does not readily accommodate prior source distributions that vary in size, shape, or location. However, the fitting procedure used in the first step of FAIR can easily handle such variations by including them as variables to be determined from the data. In the spirit of the Bayesian approach, constraints on these variables may be introduced to guide the fitting procedure toward a "reasonable" result. The use of ART in the second, iterative portion of FAIR has the disadvantage that ART tries to reduce the discrepancy in the measurement equations to zero without regard for the estimated uncertainties in the data. Thus, the FAIR result shown in Fig. 3.8-6c is quite noisy and is substantially farther from the actual source distribution (rms deviation = 0.154) than the intermediate fitted result (rms deviation = 0.031).

In a more *global Bayesian approach* to the problem, the fitting procedure in FAIR may be used to estimate suitable ensemble properties $\bar{\mathbf{f}}$ and $\mathbf{R}_f$ for input to a MAP algorithm. The fitting procedure may be viewed as defining a subensemble appropriate to the available data. This is similar to a radiologist's approach to interpreting a radiograph. The radiograph typically contains enough identifying features that the radiologist can determine which part of the body is being imaged with which imaging modality. This allows him to select the appropriate set of diagnostic criteria. For the present example, the fitting procedure used the same model as described above for the first step of FAIR and the fitted result was used for $\bar{\mathbf{f}}$. $\mathbf{R}_f$ was assumed to be 0.1 times the identity matrix. This is much smaller than the value used in the preceding MAP calculation to reflect the supposition that the fit is much closer to the desired result than the annulus of constant amplitude previously used for $\bar{\mathbf{f}}$. Figure 3.9-1 shows the MAP reconstruction using the 10% rms noise data, and the results are superior to those in Fig. 3.8-6. The rms deviation of this reconstruction relative to the source function is 0.035, whereas that for the earlier MAP result, Fig. 3.8-6, is 0.060. When this generalized MAP method is applied to the projections of the inconsistent source function shown in Fig. 3.8-4a, the result is very similar to that obtained with FAIR, Fig. 3.8-4d. These examples only hint at the power of

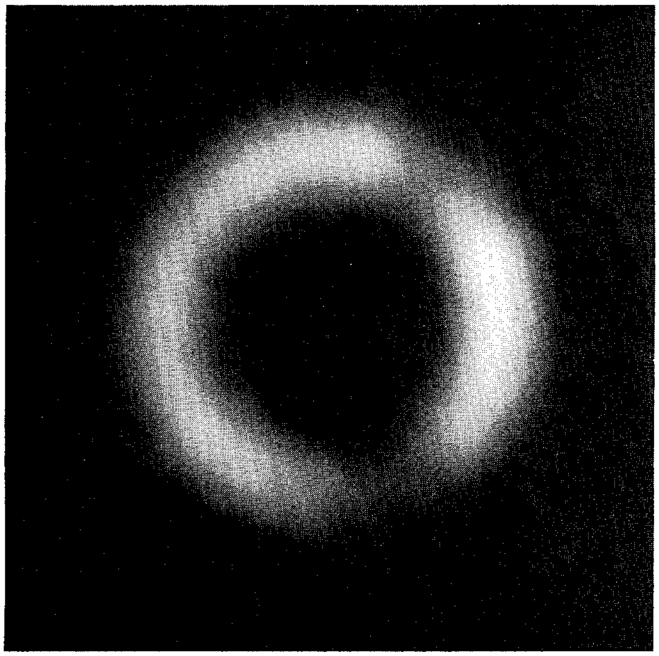

Fig. 3.9-1. Reconstruction from the same data used in Fig. 3.8-6 obtained by employing MAP as the second step in the FAIR procedure. This global Bayesian approach yields the best estimate of the original function and provides flexibility in the use of *a priori* information.

this global Bayesian approach where the MAP algorithm is used for the second, iterative step of FAIR. The true flexibility of this global approach awaits demonstration with more demanding problems.

3.10 DISCUSSION

In past comparisons of MAP results to those of more standard techniques in the areas of CT [31, 73] and in image restoration [38, 72, 88, 89], MAP yielded few or no benefits. The reasons for the success of MAP in the above limited-angle CT example problem are: (1) the solution is severely underdetermined because of the limited nature of the data set, and (2) the *a priori* assumptions about $\bar{\mathbf{f}}$ and $\mathbf{R}_f$ can be made quite restrictive because of the nature of the stated problem. It is expected that the Bayesian analysis will be most useful in situations where these two conditions hold because only then will there be both a significant contribution from the null space, which

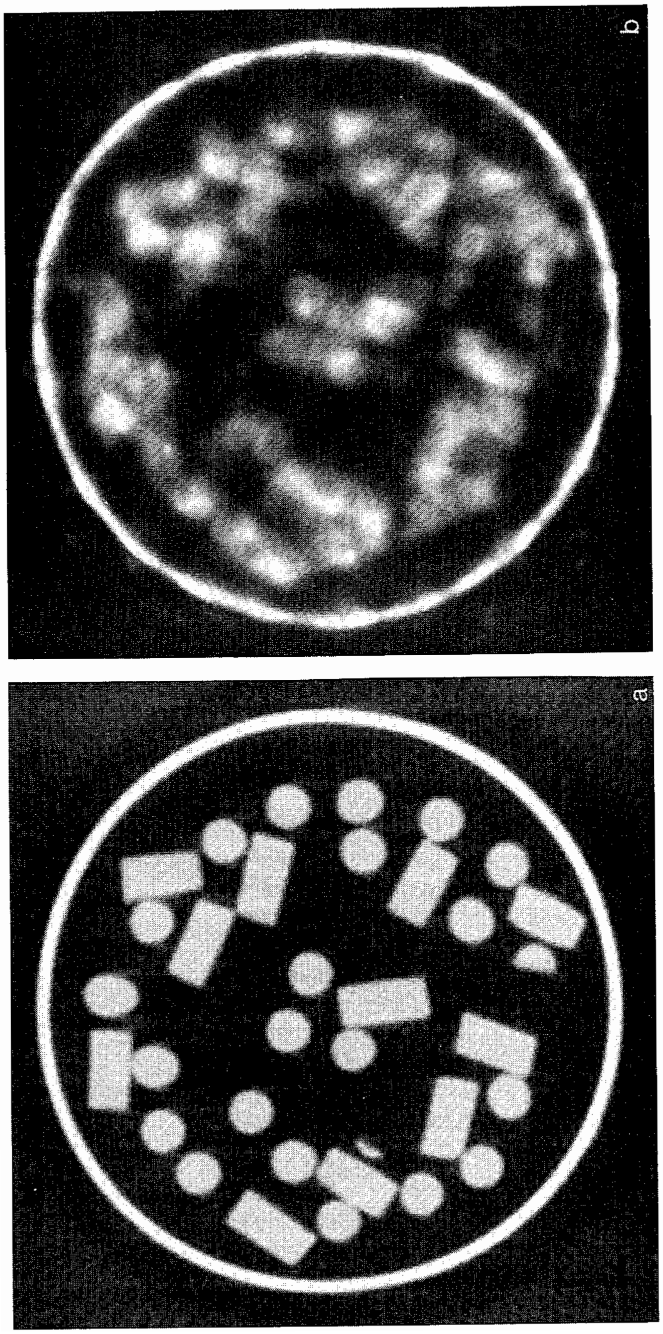
b
a

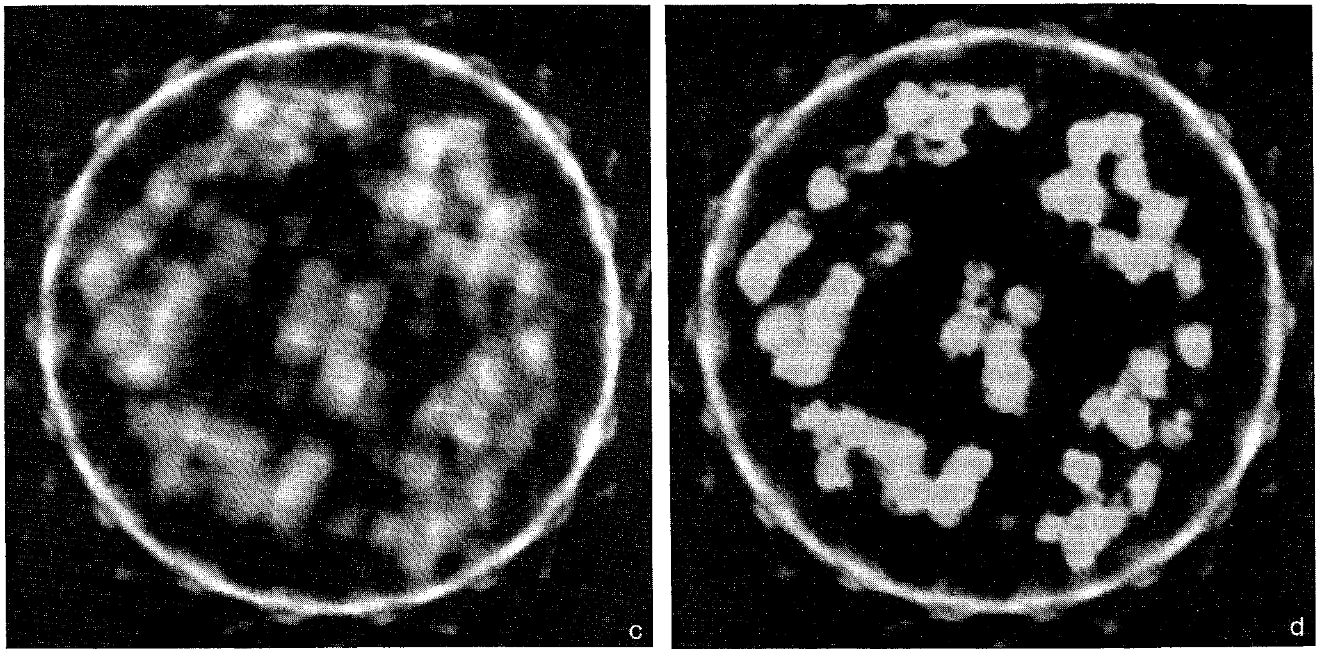

Fig. 3.10-1. Reconstructions from x-ray transmission data of a mock-up of propellant grains inside a fiberglass cannon bore. See Zoltani *et al.* [90, 91] for details. The true object is given by (a), the filtered backprojection reconstruction from 180 views. The maximum-entropy reconstructions from nine views (b) and five views (e) show artifacts similar to those in their counterparts (c) and (f) obtained by using ART with a nonnegativity constraint. The soft enforcement of binary reconstruction values in the interior of the cylinder, (d) and (g), respectively, results in ART reconstructions that are much more "reasonable". However, the reconstruction with only five views (g) is plainly wrong, even though it looks like what is expected. Incidentally, prior knowledge of the fiberglass cylinder was incorporated in (g).

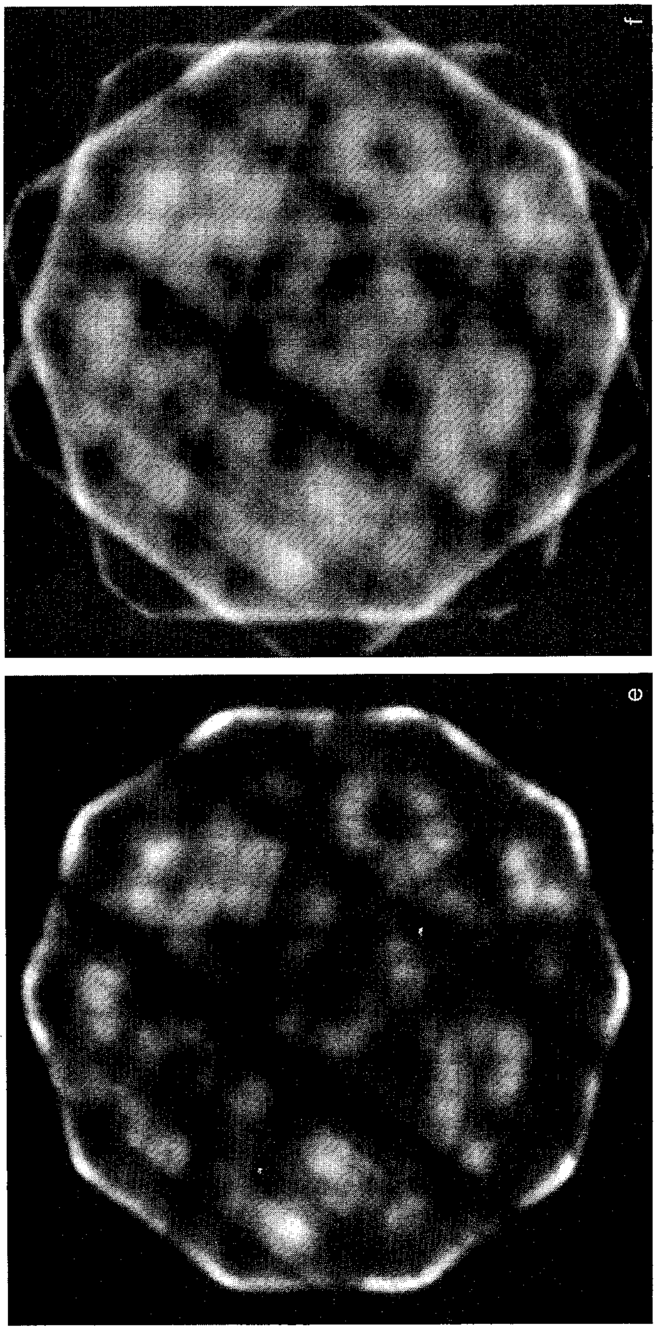
f
e

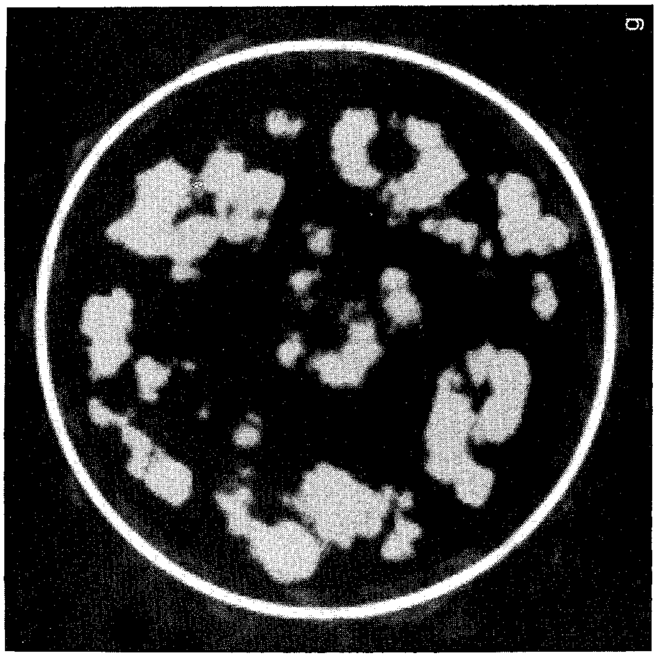

Fig. 3.10-1 (*continued*)

must be properly estimated to avoid artifacts, and the necessary information to accomplish that.

As indicated several times in this chapter, great care must be exercised in specifying the ensemble mean and covariance matrix when using the Bayesian approach. The same must be said of other supplementary forms of constraint. First, it is necessary to avoid assumptions that are inconsistent with the actual object as well as with the data. Otherwise the abundance of constraints may cause these inconsistencies to show up as artifacts that appear to be part of what was expected. The second consideration is that the MAP method necessarily produces results that are weighted toward $\bar{\mathbf{f}}$, as discussed in Section 3.4. This may not be appropriate if the sought-for entities are anomalous. The magnitude of the elements of $\mathbf{R}_f$ can be increased from their true ensemble values to allow for this. Thus one may view the selection of the ensemble characteristics as a method of "tuning" the reconstruction algorithm. This tuning must be done with the final purpose of the images kept in mind. It should be realized that this is a trade-off situation. The constraints must be restrictive in order to affect the null space and hence to reduce reconstruction artifacts. But overly restrictive constraints can obscure deviations from what one expects, which might be precisely what one is looking for. To make matters worse, in such a situation the resulting reconstructions may look very "reasonable," giving the observer a false sense of security. Figure 3.10-1shows what happens when excessively restrictive constraints (binary reconstruction values) are placed on data that possess insufficient information. This exercise suggests that the definition of an optimal reconstruction should include the ability to estimate the reliability of the interpretation from the reconstruction itself. It is this ability, among others, that distinguishes the human observer [76].

The judgment of the success of the Bayesian analysis is not a trivial process. Because the Bayesian approach is based on minimization of an ensemble variance, it can be accurately evaluated only by using a relatively large number of trials. The assessment of the technique cannot be made on the basis of a single image or even several images, as the reader of the open literature in general or of this chapter in particular is asked to do. Before a Bayesian method can be fully tested in any new imaging situation, the observers must be thoroughly trained. This requires a large set of training images for which the "truth" is known. The observer should be fully aware of the kinds of assumptions that have been made in the reconstruction process in order not to be misled by the results. Judgment of any new imaging technique is too often made on the basis of experience with past techniques without retraining the observers. Of course, such retraining is costly and demands real commitment to the new method.

3.11 SUMMARY

The deficiency in limited data is a consequence of a null space of reconstruction functions about which the available measurements say nothing. Artifacts in deterministic reconstructions can be reduced if the null-space components of the original image can be properly estimated through the use of prior information. The Bayesian approach permits the incorporation of information about the general shape or structure of the object. An iterative reconstruction algorithm is presented that finds the solution with the maximum *a posteriori* (MAP) probability. The incorporation of other kinds of prior knowledge, including maximum entropy, may be considered as special cases of the Bayesian approach. An alternative Bayesian scheme is the fit and iterative reconstruction (FAIR) algorithm that is based on a parametric model of the object, which is restricted according to prior knowledge about the object. Both MAP and FAIR are shown to work well in ameliorating reconstruction artifacts, even in the presence of noise and other sources of inconsistencies with the prior assumptions. A global Bayesian approach, which combines the flexibility of the fitting procedure in the FAIR method and the tolerance of the MAP method, promises to be even better. It is stressed that the prior constraints placed on any reconstruction must be carefully chosen so as not to automatically produce an acceptable looking result, irrespective of the data. Because the Bayesian method allows information that is not inherent in the measurement data to affect the resulting image, it is wise to take a cautious approach in interpreting its results. Thus, much personal experience with the Bayesian method is required before one can rely on it.

ACKNOWLEDGMENTS

This work was supported by the U.S. Department of Energy under contract W-7405-ENG-36. I wish to acknowledge helpful and interesting discussions with Gerald Minerbo, Michael Buonocore, Barry Medoff, Jorge Llacer, George W. Wecksung, and Henry Stark. George Wecksung is responsible for the computer codes used to generate the MAP examples shown here and for introducing me to the measurement-space/null-space concept. I thank Richard P. Kruger and Csaba Zoltani for the data used to obtain the reconstructions shown in Fig. 3.10-1.

REFERENCES

1. K. M. Hanson and G. W. Wecksung (1983). Bayesian approach to limited-angle reconstruction in computed tomography. *J. Opt. Soc. Amer.* **73**, 1501–1509.
2. K. M. Hanson, J. N. Bradbury, T. M. Cannon, R. L. Hutson, D. B. Laubacher, R. J. Macek, M. A. Paciotti and C. A. Taylor (1981). Computed tomography using proton energy loss. *Phys. Med. Biol.* **26**, 965–983.

3. K. M. Hanson, J. N. Bradbury R. A. Koeppe, R. J. Macek, D. R. Machen, R. Morgado, M. A. Paciotti, S. A. Sanford and V. W. Steward (1982). Proton computed tomography of human specimens. *Phys. Med. Biol.* **27**, 25-36.
4. A. J. Devaney (1983). A computer simulation study of diffraction tomography. *IEEE Trans. Biomed. Eng.* **BME-30**, 377-386.
5. A. J. Devaney (1984). Geophysical diffraction tomography. *IEEE Trans. Geosci. Remote Sens.* **GE-22**, 3-13.
6. H. C. Andrews and B. R. Hunt (1977). "Digital Image Restoration", Prentice-Hall, Englewood Cliffs, New Jersey.
7. K. T. Smith, D. C. Solmon and S. L. Wagner (1977). Practical and mathematical aspects of the problem of reconstructing objects from radiographs. *Bull. Amer. Math. Soc.* **83**, 1227-1270.
8. S. Twomey (1965). The application of numerical filtering to the solution of integral equations encountered in indirect sensing measurement. *J. Frank Inst.* **279**, 95-109.
9. S. Twomey and H. B. Howell (1967). Some aspects of the optical estimation of microstructure in fog and cloud. *Appl. Opt.* **6**, 2125-2131.
10. S. Twomey (1974). Information content in remote sensing. *Appl. Opt.* **13**, 942-945.
11. K. Tanabe (1971). Projection method for solving a singular system of linear equations and its applications. *Numer. Math.* **17**, 203-214.
12. D. D. Jackson (1972). Interpretation of inaccurate, insufficient and inconsistent data. *Geophys. J. R. Astr. Soc.* **28**, 97-109.
13. M. B. Katz (1979). "Questions of Uniqueness and Resolution in Reconstruction from Projections," Lecture Notes in Biomathematics, (S. Levin, ed.) Springer, Berlin.
14. J. Llacer (1979). Theory of imaging with a very limited number of projections. *IEEE Trans. Nucl. Sci.* **NS-26**, 596-602.
15. J. L. C. Sanz and T. S. Huang (1983). Unified Hilbert space approach to iterative least-squares linear signal restoration. *J. Opt. Soc. Am.* **73**, 1455-1465.
16. R. Gordon, R. Bender and G. T. Herman (1970). Algebraic reconstruction techniques for three-dimensional electron microscopy and x-ray photography. *J. Theor. Biol.* **29**, 471-481.
17. B. F. Logan and L. A. Shepp (1975). Optimal reconstruction of a function from its projections. *Duke Math. Jour.* **42**, 645-659.
18. A. V. Lakshminarayan and A. Lent (1976). The simultaneous iterative reconstruction technique as a least-squares method. *Proc. SPIE* **96**, 108-116.
19. C. Hamaker and D. C. Solmon (1978). The angles between the null spaces of x rays. *J. Math. Anal. Appl.* **62**, 1-23.
20. A. K. Louis (1981). Ghosts in tomography—The null space of the Radon transform. *Math. Meth. Appl. Sci.* **3**, 1-10.
21. A. K. Louis (1984). Orthogonal function series expansions and the null space of the Radon transform. *SIAM J. Math. Anal.* **15**, 621-633.
22. B. P. Medoff, W. R. Brody and A. Macovski (1982). Image reconstruction from limited data. *Proc. Int. Workshop on Physics and Engineering in Medical Imaging*, Pacific Grove, 1982, IEEE Computer Society, Silver Spring, 188-192.
23. B. P. Medoff, W. R. Brody, M. Nassi and A. Macovski (1983). Iterative convolution backprojection algorithms for image reconstruction from limited data. *J. Opt. Soc. Am.* **73**, 1493-1500.
24. K. M. Hanson (1982). CT reconstruction from limited projection angles. *Proc. SPIE* **347**, 166-173.
25. Buonocore, M. H., Brody, W. R., and Macovski, A. (1981). Natural pixel decomposition for two-dimensional image reconstruction. *IEEE Trans. Biomed. Eng.* **BME-28**, 69-78.
26. G. T. Herman (1980), "Image Reconstruction from Projections," Academic Press, New York.

27. Shepp, L. A., and Logan, B. F. (1974). The Fourier reconstruction of a head section. *IEEE Trans. Nucl. Sci.* **NS-21**, 21–43.
28. R. Gordon (1974). A tutorial on ART. *IEEE Trans. Nucl. Sci.* **NS-21**, 78–93.
29. P. Gilbert (1972). Iterative methods for the three-dimensional reconstruction of an object from projections. *J. Theor. Biol.* **36**, 105–117.
30. M. Goitein (1972). Three-dimensional density reconstruction from a series of two-dimensional projections. *Nucl. Instrum. Meth.* **101**, 509–518.
31. G. T. Herman and A Lent (1976). A computer implementation of a Bayesian analysis of image reconstruction. *Inform. Contr.* **31**, 364–384.
32. K. M. Hanson and G. W. Wecksung (1985). Local basis-function approach to computed tomography. *Appl. Opt.* **24**, 4028–4039.
33. A. Ben Israel and T. N. E. Greville (1974). "Generalized Inverses: Theory and Applications," John Wiley and Sons, New York, pp. 244–245.
34. D. G. McCaughey and H. C. Andrews (1977). Degrees of freedom for projection imaging. *IEEE Trans. Acoust., Speech, Signal Processing* **ASSP-25**, 63–73.
35. T. M. Cannon (1976). Blind deconvolution of spatially invariant image blurs with phase. *IEEE Trans. Accoust., Speech, Signal Processing* **ASSP-24**, 58–63.
36. D. C. Ghiglia (1984). Space-invariant deblurring given N independent blurred images of a common object. *J. Opt. Soc. Am.* **A1**, 398–402.
37. A. P. Sage and J. L. Melsa (1979). "Estimation Theory with Applications to Communications and Control," Robert E. Krieger, Huntington, p. 175.
38. B. R. Hunt (1977). Bayesian methods in nonlinear digital image restoration. *IEEE Trans. Comput.* **C-26**, 219–229.
39. G. T. Herman and A. Lent (1976). Iterative reconstruction algorithms. *Comput. Biol. Med.* **6**, 273–294.
40. P. R. Bevington (1969). "Data Reduction and Error Analysis for the Physical Sciences," McGraw-Hill, New York.
41. B. R. Frieden (1972). Restoring with maximum likelihood and maximum entropy. *J. Opt. Soc. Am.* **62**, 511–518.
42. L. A. Shepp and Y. Vardi (1982). Maximum likelihood reconstruction for emission tomography. *IEEE Trans. Med. Imaging* **MI-1**, 113–122.
43. T. Inouye (1979). Image reconstruction with limited-angle projection data. *IEEE Trans. Nucl. Sci.* **NS-26**, 2666–2669.
44. T. Inouye (1982). Image reconstruction with limited view angle projections. *Proc. Int. Workshop on Physics and Engineering in Medical Imaging*, Pacific Grove, 1982, IEEE Computer Society, Silver Spring, Maryland, 165–168.
45. A. M. Cormack (1963). Representation of a function by its line integrals, with some radiological applications. *J. Appl. Phys.* **34**, 2722–2727, and *J. Appl. Phys.* **35**, 2908–2913.
46. K. C. Tam, V. Perez-Mendez and B. Macdonald (1979). 3-D object reconstruction in emission and transmission tomography with limited-angular input. *IEEE Trans. Nucl. Sci.* **NS-26**, 2797–2805.
47. R. W. Gerchberg (1974). Super-resolution through error energy reduction. *Opt. Acta* **21**, 709–720.
48. A. Papoulis (1975). A new algorithm in spectral analysis and band-limited extrapolation. *IEEE Trans. Circuits Syst.* **CAS-22**, 735–742.
49. K. C. Tam and V. Perez-Mendez (1981). Tomographic imaging with limited-angle input. *J. Opt. Soc. Am.* **71**, 582–592.
50. K. C. Tam and V. Perez-Mendez (1981). Limits to image reconstruction from restricted angular input. *IEEE Trans. Nucl. Sci.* **NS-28**, 179–183.
51. F. A. Grünbaum (1980). A study of Fourier space methods for limited-angle image reconstruction. *Numer. Funct. Anal. and Optimiz.* **2**, 31–42.

52. T. Sato, S. J. Norton, M. Linzer, O. Ikeda and M. Hirama (1981). Tomographic image reconstruction from limited projections using iterative revisions in image and transform spaces. *Appl. Opt.* **20**, 395–399.
53. M. H. Buonocore, W. R. Brody and A. Macovski (1981). Fast minimum variance estimator for limited-angle CT image reconstruction. *Med. Phys.* **8**, 695–702.
54. T. S. Huang, D. A. Barker and S. P. Berger (1975). Iterative image restoration. *Appl. Opt.* **14**, 1165–1168.
55. R. W. Schafer, R. M. Mersereau and M. A. Richards (1981). Constrained iterative restoration algorithms. *Proc. IEEE* **69**, 432–450.
56. M. I. Sezan and H. Stark (1982). Image restoration by the method of convex projections: Part 2—Applications and numerical results. *IEEE Trans. Med. Imag.* **MI-1**, 95–101.
57. S. F. Burch, S. F. Gull and J. Skilling (1983). Image restoration by a powerful maximum entropy method. *Comp. Vision Graphics Image Process.* **23**, 113–128.
58. H. J. Trussell and M. R. Civanlar (1984). The feasible solution in signal restoration. *IEEE Trans. Acoust., Speech, Signal Processing* **ASSP-32**, 201–212.
59. K. M. Hanson (1986). Effect of nonnegativity constraints on detectability. *Proc. Topical Meeting on Quantum Limited Imaging and Image Processing*, Honolulu, 1986 (Opt. Soc. Am.) (to be published elsewhere).
60. D. C. Youla and H. Webb (1982). Image restoration by the method of convex projections: Part 1—Theory. *IEEE Trans. Med. Imag.* **MI-1**, 81–94.
61. H. J. Trussell and M. R. Civanlar (1985). Digital signal restoration using projection and fuzzy set techniques (submitted to *IEEE Trans. Acoust., Speech, Signal Processing*).
62. S. J. Wernecke and L. R. d'Addario (1977). Maximum entropy image restoration. *IEEE Trans. Comput.* **C-26**, 351–364.
63. S. F. Gull and G. J. Daniell (1978). Image reconstruction from incomplete and noisy data. *Nature* **272**, 686–690.
64. G. Minerbo, G. (1979). MENT: A maximum entropy algorithm for reconstructing a source from projection data. *Comput. Graph. Imag. Process.* **10**, 48–68.
65. H. J. Trussell (1980). The relationship between image reconstruction by the maximum *a posteriori* method and a maximum entropy method. *IEEE Trans. Acoust., Speech, Signal Processing* **ASSP-28**, 114–117.
66. J. Skilling (1984). Theory of maximum entropy image reconstruction. *Proc. 4th Workshop on Maximum Entropy and Bayesian Methods in Applied Statistics*, Calgary, 1984 (J. H. Justice, ed.), Cambridge University Press, Cambridge, England.
67. J. E. Shore and R. W. Johnson (1980). Axiomatic derivation of maximum entropy and the principle of minimum cross-entropy. *IEEE Trans. Inform. Theory* **IT-26**, 26–37.
68. B. R. Musicus (1983). Iterative algorithms for optimal signal reconstruction and parameter identification given noisy and incomplete data. *Proc. Int. Conf. Acoust., Speech, Signal Processing*, Boston, 1983.
69. D. M. Titterington (1984). The maximum entropy method for data analysis. *Nature* **312**, 381–382.
70. R. Nityananda and R. Narayan (1982). Maximum entropy image reconstruction—A practical noninformation-theoretic approach. *J. Astrophys. Astr. (India)* **3**, 419–450.
71. T. J. Ponman (1984). Maximum entropy methods. *Nucl. Instru. Meth.* **221**, 72–76.
72. H. J. Trussell and B. R. Hunt (1979). Improved methods of maximum *a posteriori* restoration. *IEEE Trans. Comput.* **C-27**, 57–62.
73. G. T. Herman, H. Hurwitz, A. Lent and H. Lung (1979). On the Bayesian approach to image reconstruction. *Inform. Contr.* **42**, 60–71.
74. K. M. Hanson (1984). Tomographic reconstruction of axially symmetric objects from a single radiograph. *Proc. SPIE* **491**, 180–187.

75. K. M. Hanson (1985). A Bayesian approach to nonlinear inversion: Abel inversion from x-ray attentuation data, presented at the *Fourth Workshop on Maximum Entropy and Bayesian Methods in Applied Statistics*, Calgary, 1984 (to be published elsewhere).
76. K. M. Hanson (1985). Image processing: Mathematics, engineering, or art? *Proc. SPIE* **535**, 70-81.
77. S. Kaczmarz (1937). Angenährte Auflösung von Systemen linearer Gleichungen. *Bull. Int. Acad. Pol. Sci. Lett.* **A**, 355-357.
78. H. J. Trussell and M. R. Civanlar (1985). The Landweber iteration and projection onto convex sets. *IEEE Trans. Acoust., Speech, Signal Processing* **ASSP-33**, 1632-1633.
79. S. L. Wood, A. Macovski and M. Morf (1979). Reconstructions with limited data using estimation theory. In "Computer Aided Tomography and Ultrasonics in Medicine," (J. Raviv, J. F. Greenlead, G. T. Herman, eds.), *Proc. IFIP, TC-4 Working Conf.,* Haifa, Israel, 1978, North-Holland, Amsterdam, 219-233.
80. S. L. Wood and M. Morf (1981). A fast implementation of a minimum variance estimator for computerized tomography image reconstruction. *IEEE Trans. Biomed. Eng.* **BME-28**, 56-68.
81. W. E. Smith, H. H. Barrett and R. G. Paxman (1983). Reconstruction of objects from coded images by simulated annealing. *Opt. Lett.* **8**, 199-201.
82. W. E. Smith, R. G. Paxman and H. H. Barrett (1985). Image reconstruction from coded data: I. Reconstruction algorithms and experimental results. *J. Opt. Soc. Am.* **A2**, 491-500.
83. S. Geman and D. Geman (1984). Stochastic relaxation, Gibbs distributions, and the Bayesian restoration of images. *IEEE Trans. Pattern Anal. Machine Intell.* **PAMI-6**, 721-741.
84. G. R. Gindi, R. G. Paxman and H. H. Barrett (1984). Reconstruction of an object from its coded image and object constraints. *Appl. Opt.* **23**, 851-856.
85. K. M. Hanson (1982). Limited-angle CT reconstruction using *a priori* information. *Proc. First IEEE Computer Society Int. Sympt. on Medical Imaging Interpretation*, Berlin, 1982, IEEE Computer Society, Silver Spring, Maryland, 527-533.
86. Y. Censor, P. P. B. Eggermont and D. Gordon (1983). Strong underrelaxation in Kaczmarz's method for inconsistent systems. *Numer. Math.* **41**, 83-92.
87. M. T. LeFree, R. A. Vogel, D. L. Kirch and P. P. Steele (1981). Seven-pinhole tomography—A technical description. *J. Nucl. Med.* **22**, 48-54.
88. H. J. Trussell (1978). Notes on linear image restoration by maximizing the *a posteriori* probability. *IEEE Trans. Comp.* **C-27**, 57-62.
89. T. M. Cannon, H. J. Trussell and B. R. Hunt (1978). Comparison of image restoration methods. *Appl. Opt.* **17**, 3384-3390.
90. C. K. Zoltani, K. J. White and R. P. Kruger (1983). Results of feasibility study on computer assisted tomography for ballistic applications. *Tech. Report ARBRL-TR-02513*, Ballistic Research Laboratory, Aberdeen Proving Ground, Maryland.
91. C. K. Zoltani, K. J. White and F. A. DiBianca (1986). The flash x-ray computed tomography facility for microsecond events (to be published in *Rev. Sci. Instr.*).